KfK 4256
Mai 1987

The SANDCMOT Sodium Boiling Model

P. R. Henkel
Institut für Neutronenphysik und Reaktortechnik
Projekt Schneller Brüter

Kernforschungszentrum Karlsruhe

KERNFORSCHUNGSZENTRUM KARLSRUHE

Institut für Neutronenphysik und Reaktortechnik
Projekt Schneller Brüter

KfK 4256

The SANDCMOT sodium boiling model

P. R. Henkel

Kernforschungszentrum Karlsruhe GmbH, Karlsruhe

Kernforschungszentrum Karlsruhe GmbH
Postfach 3640, 7500 Karlsruhe 1

ISSN 0303-4003

The SANDCMOT sodium boiling model

Abstract

This report describes the sodium boiling model that recently was incorporated into the SANDCMOT code. This code was previously used for clad motion analysis of unprotected loss of flow (ULOF) accidents in LMFBR's. The chosen boiling model is an unstructered flow model that uses three conservation equations (mass, momentum, enthalpy) for a mixture flow. Furthermore, thermodynamic equilibrium of the two phases is assumed along the saturation line. Mechanical disequilibrium, however, is allowed and described by a slip correlation. As SANDCMOT considers several subchannels that are connected radially, the boiling model is two dimensional (r,z geometry). A first step of verification work was done by recalculating the TREAT-R5 experiment.

Das SANDCMOT Natriumsiedemodell

Zusammenfassung

In diesem Bericht wird das Natriumsiedemodell beschrieben, das kürzlich in das Programm SANDCMOT integriert wurde. Das Programm wurde zuvor schon zur Analyse der Hüllrohrmaterialbewegung in unkontrollierten Kühlmitteldurchsatzstörfällen in Schnellen Brutreaktoren benutzt. Das gewählte Siedemodell enthält ein unstrukturiertes Strömungsmodell, das drei Erhaltungsgleichungen (für Masse, Impuls und Enthalpie) löst. Weiterhin wird thermodynamisches Gleichgewicht der zwei Phasen entlang der Sättigungskennlinie angenommen. Mechanisches Nichtgleichgewicht ist jedoch erlaubt und wird durch eine Schlupfbeziehung beschrieben. Da in SANDCMOT mehrere Unterkanäle betrachtet werden, die radial miteinander verbunden sind, ist das Siedemodell zweidimensional (r,z Geometrie) ausgelegt. Ein erster Schritt zur Verifizierung des Modells wurde durch die Nachrechnung des TREAT-R5 Experiments unternommen.

Table of contents

List of figures

1. Introduction

Within the frame of LMFBR safety analysis unprotected loss of flow (ULOF) accidents are investigated. These accidents are characterized by a thermal unbalance resulting from the continued power production within the reactor core and an increasingly less effective cooling system due to the flow rate reduction. If complete failure of the two independent reactor shut-down systems is assumed such a situation inevitably will lead to sodium boiling , dry-out of fuel pins, their overheating and final failure. There are several possible failure scenarios depending essentially on the reactor power during the boiling phase. If by sodium voiding the reactivity is only slightly increased the reactor power stays near nominal and clad melting and motion will be initiated within about 1-2 seconds after dry-out. Fuel melting and motion will start after several seconds only. Such accident evolutions are likely for small or heterogeneous cores. If on the other hand the sodium void reactivity is relatively high as this is the case in large reactor cores, power will raise rapidly and lead to simultaneous melting of fuel and cladding. A mixture flow of these pin materials together with eventually available fission products will develop. This situation is very different to the case considered first. There, it is likely that clad relocation will take place independently of fuel motion within a more or less intact pin bundle geometry. Experiments show that a denuded fuel pellet column still has a considerable stability and can preserve its integrity for quite a while.

For these situations, a multichannel clad relocation model has been developed at KfK for several years/1/. As it requires initial state and extensive boundary data it was incorporated into the host code SANDPIN/3/. This code has a pin model to determine the transient temperature distribution within fuel and cladding, a fission gas and a mechanics (stress/strain) model. A sodium boiling model, however, was not included, yet. In order to achieve more flexibility and to make the code also suitable for realistic initiation phase calculations of LOF accidents the sodium boiling model to be described hereafter was incorporated. In its current form the code may well be used for analysis of boiling and clad motion scenarios. The basic annular ring geometry allows to represent hexagonal (or any symmetrical) pin

bundles if certain cluster of pins are lumped together to an annular ring. Radial cross flows between the major coolant channels are also modelled.

The choice of a specific boiling model was governed by the need to fit the general methodology and numerical solution technique of SANDCMOT. For sodium boiling essentially two basic approaches exist. There are so called structured flow models that consider single vapor bubbles and descibe their dynamics and interaction with neighboring liquid slugs. A successful representative of this line is the BLOW3A code /4/. A completely different approach is derived from water boiling models and considers a two phase homogeneous mixture flow. For this flow the conservation equations are solved. This latter way is followed here because of its suitability to the SANDCMOT solution scheme. Several different mixture flow models can be obtained depending on how many conservation equations are solved and which simplifications are made. In SANDCMOT the mixture conservation equations of mass, momentum and enthalpy are solved under the assumption of thermodynamic equilibrium along the saturation line. Mechanical disequilibrium between the phases (a certain slip) is however allowed. This slip is calculated from the Chrisholm relation /5/. The first assumption is justified by the high thermal conductivity of liquid sodium that will keep temperature differences small. The allowed slip is essential because vapor and liquid densities differ by about a facor of 1000. This may result in high vapor velocities of order 100 m/s while those of the liquid are still low (less than 10 m/s). Such differences are important for pressure drop predictions and influence the characteristic oscillations common to sodium boiling processes.

In the following chapters the basic conservation equations and constitutive relations are presented. Next, the numerical solution method is explained. Finally, the results obtained from a recalculation of the TREAT-R5 experiment are shown.

II. The three equation mixture model

II.1 Conservation equations

The current mixture flow model is based on three conservation equations that are obtained by summation of the basic balance equations of each phase. For later use, several definitions are in place. The void fraction α is defined locally as the ratio of vapor volume to some reference volume which, in our case is the coolant channel volume (e.g. cross section multiplied by a reference axial height).

$$\alpha = V_g/V_{ref} = A_g/A_{ref} \tag{2.1a}$$

A mixture density and enthalpy is defined by

$$\rho = \alpha\rho_v + (1-\alpha)\rho_l \tag{2.1b}$$

$$h = (\alpha\rho_v h_v + (1-\alpha)\rho_l h_l)/\rho$$

where the phasic quantities are evaluated at the local saturation temperature. Also, the mass flux density vector Γ is given by

$$\Gamma = (\alpha\rho_v W_v + (1-\alpha)\rho_l W_l) = (G_r, G_z)^T$$

Here, W means the velocity vector including an axial (v) and radial (u) component, $W = (u,v)^T$. The slip factor S is taken as a direction independent quantity and is defined by

$$W_v = S\, W_l \tag{2.1c}$$

Based on these definitions the vapor quality x can be expressed as

$$\alpha\rho_v W_v = \Gamma_v = x\,\Gamma \qquad \text{(definition)} \tag{2.1d}$$

$$x = \alpha\rho_v S/(\alpha\rho_v S + (1-\alpha)\rho_l)$$

In turn, the void fraction α may be specified in terms of x and S

$$\alpha = x\rho_l/(x\rho_l + (1-x)\rho_v S)$$

The basic conservation laws of mixture mass, momentum and enthalpy can be stated as follows :

Continuity

$$\delta/\delta t\ \rho + \nabla\ (\alpha\rho_v W_v + (1-\alpha)\rho_l W_l) = 0 \qquad (2.1e)$$

Momentum

$$\delta/\delta t\ \Gamma + \nabla\ (\alpha\rho_v W_v W_v + (1-\alpha)\rho_l W_l W_l) + \nabla\ p + \rho g + F_w = 0$$

Enthalpy

$$\delta/\delta t\ \rho h + \nabla\ (\alpha\rho_v h_v W_v + (1-\alpha)\rho_l h_l W_l) - d/dt\ p + \nabla\ q = Q_w$$

In above equations, p is the pressure unique to both phases. This choice ignores any interfacial effects for example due to surface tension. g is the acceleration vector having a non-vanishing component only in axial direction. Also, F_w denotes the wall friction force vector per unit of volume. Its radial component describes the friction of the radial flow across the pin matrix. Furthermore, q denotes the fluid heat flux vector and Q_w is the power input by heat conduction from the fuel pins. Finally, the symbol d/dt means the total time derivative $\delta/\delta t + (\alpha W_v + (1-\alpha)W_l)\nabla$ that is constructed with an average velocity of the two-phase mixture.

There are a total of twelve unknowns appearing in eqs. (2.1e). These are the void fraction α, pressure p, densities ρ, ρ_v, ρ_l, enthalpies h, h_v, h_l and the two components of the vector quantities W_v and W_l. The wall friction force and the heat source term are assumed to depend on these variables as well as on the phase temperatures by constitutive relations. Including T_v, T_l, one is left with fourteen

unknowns. On the other hand, eqs. (2.1a-d) and (2.1e) constitute a set of eight equations. The required additional relationships are provided by the equations of state

$$\rho_v = \rho_v(p,T_v) \tag{2.1f}$$

$$\rho_l = \rho_l(p,T_l)$$

$$h_v = h_v(p,T_v)$$

$$h_l = h_l(p,T_l)$$

Additionally, the thermodynamic equilibrium assumption gives

$$T_v = T_l = TSAT(p) \tag{2.1g}$$

where TSAT denotes the saturation temperature corresponding to pressure p. Thus, also fourteen equations are available that may serve to solve for the unknowns. If p, h and Γ are taken as the main variables and have been calculated already the other variables merely follow by definition.

I.2 Characteristics

In order to make the first order partial differential equation system (FOPDE) (2.1e) (together with appropriate initial and boundary conditions) a well-posed initial value problem the characteristics have to be all real /16/. For the case of no interphase slip (S = 1), this property can indeed be proved. As the characteristics are all different the system is hyperbolic. The proof can be found in ref./16/. If there is some slip an analogue characteristics analysis can be carried out. In Appendix D the characteristic polynomial is derived. However, the question if only real solutions do exist is not settled because the general solution is not found. Some remarks can be given, however. As the mixture flow equation system is derived from

the conservation equations of each phase it is worthwile to consider their characteristics problem. The authors of ref. /16/ as well as Stewart and Wendroff /17/ show that the so-called basic model including three conservation equations for each phase under the assumption of a unique pressure within both phases has complex characteristics provided the relative velocity of the two phases 1 and 2 fulfills the inequalities

$$0 < (u_1 - u_2)^2 < (c_1 c_2)^2 \, Z \, / \, (\rho_2 \alpha_1 c_2^{\,2} + \rho_1 \alpha_2 c_1^{\,2})$$

$$Z = (\rho_1 \alpha_2)^{1/3} + (\rho_2 \alpha_1)^{1/3}, \quad (c_i)^{-2} = \delta \rho_i / \delta p \qquad (2.1h)$$

Thus, for moderate relative velocities some roots are complex. The situation changes if additional transient flow force terms (virtual mass terms) are included. These terms may provide additional derivatives that alter the characteristics. Inclusion of a term $A_m \, \delta/\delta t(v_1 - v_g)$ may indeed remove large portions of the complex solution space /16/.

In mixture flow models interfacial friction terms cancel out in the basic mixture conservation equations. They are, however, implicitly present in the specific slip correlation chosen . Therefore, it will depend strongly on this choice if our mixture flow model will have real characteristics.

An initial value problem with complex characteristics is mathematically ill-posed. Finite difference schemes that are consistent with the differential equations are unstable /16/. Despite these shortcomings numerical schemes exist that can arrive at stable and still accurate solutions. This phenomenon is associated with the finite difference approximation along a chosen spatial mesh that does not allow to represent high frequency modes. As these high frequency modes are responsible for uncontrolled growth they may be eliminated by a not too fine spatial mesh. The other modes then may be stabilized by sufficient damping, either numerical or physical. Thus well-behaved solutions may be insured. The above reasoning essentially follows the one given in ref. /7/ where some more considerations about ill-posed problems can be found.

II.2 Constitutive equations

Most of any model's physical content is brought in by the specific choice of constitutive relations. Especially the wall friction forces, the slip ratio of the phasic velocities and the heat source term are of major importance. All these quantities strongly depend on the actual flow regime. As no rigorous quantitative treatment of flow regimes exists a great deal of empiricism is introduced via the constitutive relations. The final justification for a specific choice lies in the models capability to display reasonable results for the experiments in question.

2.1 Wall friction

The friction force (per unit of volume) experienced by the fluid at the pin surfaces is calculated from a standard single phase expression plus a correction due to two-phase flow. This correction is determined according to the Lockhart- Martinelli approach. If flow in axial direction is considered first, the single phase expression is

$$F_w = f_{sp}\, G|G|/2\rho D_h \qquad (2.2a)$$

Here, f_{sp} is the single phase friction factor, G the one-dimensional mass flux and D_h the hydraulic diameter. f_{sp} depends on whether the flow is laminar or turbulent. It is assumed to have the general form

$$f_{sp} = a/Re^b \;,\; Re = |GD_h/\mu| \qquad (2.2b)$$

with

$a = 64.$, $b = 1.$ $\quad Re < Re_{crit}$

$a = 0.316$, $b = 0.25$ $\quad Re_{crit} < Re < 10^4$

$a = 0.046$, $b = 0.2$ $\quad Re > 10^4$

$Re_{crit} = 2300.$

Of course, the Reynoldsnumber is calculated with either the liquid or vapor phase flow rate and dynamic viscosity.

If the flow is two phase it is first decided which phase is dominating the flow. This is done in dependence of the vapor quality x. If x is less than 0.5 the flow is assumed to be mainly due to liquid, otherwise due to vapor. Then the corresponding single phase friction factor is calculated and a two-phase friction multiplier Ψ^2 is determined. In case of a dominant liquid flow the wall friction force is given by

$$F_w = f_{sp,l}\, G|G|(1-x)^2\, \Psi_l^2 /2\rho_l D_h \qquad (2.2c)$$

where G now is the total mass flow rate as defined in (2.1). Similarly, if the flow is mainly due to vapor the wall friction force is derived from

$$F_w = f_{sp,v}\, G|G|x^2\, \Psi_v^2 /2\rho_v D_h$$

The two-phase multipliers Ψ_l^2 and Ψ_v^2 depend on the so called Lockhart-Martinelli flow parameter X_{tt} :

$$X_{tt} = (1/x-1)^{0.9}\, (\rho_v/\rho_l)^{0.5}\, (\mu_l/\mu_v)^{0.1} \qquad (2.2d)$$

The index tt indicates that both phases are assumed to be in turbulent flow. A somewhat modified form holds for one or both phases laminar but this case probably is rather seldom and is currently not considered. The functional dependence of $\Psi^2_{l,v}$ on X_{tt} has been taken from ref. /6/

$$\Psi_l^2 = 1 + C/X_{tt} + X_{tt}^{-2}$$

$$\Psi_v^2 = 1 + C\, X_{tt} + X_{tt}^{2}$$

For axial flow the recommended value of C is 20. Other formulations are also available and may prove to be better suited for differing

applications of the code. Some are given in the description of the THERMIT code /7/ developed for analysis of light water reactor cores.

The transverse friction force is derived in a similar way as for the axial flow case. The formulation is adopted from the THERMIT-code and uses a single phase friction factor proposed by Gunter and Shaw /8/ for flow across a tube bank. The transverse hydraulic diameter is defined by

$$D_{h,tr} = 4 \text{ x free volume in tube bank / friction surface area}$$

and the radial Reynoldsnumber by $Re_r = |G_r D_{h,tr}/\mu|$. Here, G_r is the total radial mass flow rate and μ the dynamic viscosity of either phase depending on which one is mainly carrying the flow. The single phase friction factor is given by

$$f_{sp,r} = \begin{cases} 180./Re_r & Re_r < Re^* \\ 1.92/(Re_r)^{**}0.145 & Re_r < Re^* \end{cases} \qquad (2.2e)$$

and $Re^* = 202.5$. In case of two-phase flow the same multipliers as above are used but with a recommended value of C = 8.

It should be mentioned that SANDCMOT also includes form pressure drops due to axial flow area changes and irreversible flow redistributions. These may be caused by spacer grids which can be modelled in SANDCMOT (see chapter on geometry) or by clad motion in a later stage of the loss of flow accident. The form pressure drop determination is adopted from the PLUGM-code /9/ and strictly valid only for single phase flow. It is distinguished between flow contractions and expansions in dependence of the flow direction. Also, for the TREAT-R5 experiment it was essential to model the pressure drop in the piping system connected to the core in order to describe correctly the flow coast down. To this purpose pressure drops were located at the core inlet and exit. Their detailed form will be given when the TREAT-R5 experiment is discussed.

2.2 Slip ratio

As the liquid and vapor densities may differ by more than a factor of thousand, a considerable slip between the two phases is possible. As this may have an essential influence on the pressure drop the relative slip was taken into account. An empirical correlation due to Chrisholm /5/ is used to describe this slip

$$S = (1 - x + x\rho_l/\rho_v)^{1/2} \qquad (2.2f)$$

In order to assure stability the slip ratio was limited to a certain maximum value. For the TREAT-R5 experiment, S_{max} was chosen to be 30. This value allowed vapor velocities up to 200. m/s which probably is a reasonable upper limit to vapor velocities.

2.3 Energy source term Q_w

During a loss of flow accident the coolant is heated up mainly by heat conduction from the fuel pins. The corresponding heat flux ϕ from the clad surface to the coolant may be expressed as

$$\phi = h_w (T_w - T_{cool}) \qquad (2.2g)$$

T_w is the clad surface temperature or eventually the surface temperature of some structure wall. T_{cool} denotes the coolant temperature and h_w is a general heat transfer coefficient. It strongly depends on the various flow regimes possible in two-phase flow. Its value may differ drastically depending on whether one has single phase liquid convection, subcooled or saturated boiling, critical heat flux conditions, film boiling or vapor convection. Sodium boiling usually is characterized by the development of large vapor bubbles leaving only a small liquid film on the pins. This liquid film still provides efficient cooling to the pins but is diminished due to vaporization and entrainment. Also, developping disturbance waves ('roll-waves') may cause film thinning and early dry-out. Nucleate boiling usually leads to an increase in heat transfer but is probably of less

importance in sodium boiling situations compared to water given the high heat conductivity of liquid sodium. Because of the prevailing annular flow regime the liquid convection heat transfer mechanism was assumed to dominate up to critical heat flux conditions. Nucleate boiling is currently not included. If necessary a treatment as proposed in /10/ is possible. There, nucleate boiling heat transfer is estimated including results of Forster and Zuber /11/ and of Chen /12/.

Concerning the sodium liquid convection heat transfer the user has two options. One is the Lyon correlation (see /13/)

$$h_{w,l} = (7.0 + 0.021\ Re^{0.8}\ Pr^{0.8})\ k_l/D_h$$

The Reynolds number is calculated based on the total axial mass flow rate. Pr is the Prandtl number and k_l the heat conductivity. The second option available is the so called FFTF correlation :

$$h_{w,l} = (5.85 + 0.021\ Re^{0.8}\ Pr^{0.8})\ k_l/D_h \qquad (2.2h)$$

developed primarily for the FFTF reactor.

When the critical heat flux condition is reached above formulas are not appropriate any more. Then convective heat transfer to the vapor flow is important. It is described by the widely-used Dittus-Boelter formula

$$h_{w,v} = (0.023\ Re^{0.8}\ Pr^{0.33})\ k_v/D_h \qquad (2.2i)$$

It is essential to note that the thermal conductivity k_v of sodium vapor is significantly less than that for the liquid phase (about a factor of 1000.)

One more detail is important. When the critical heat flux is reached but the liquid flow rate is not zero the liquid is assumed to flow in form of droplets. These eventually may impinge onto the pins and contribute to some cooling while enforcing their own evaporation. This effect has been taken into account by adding a componet $h_{w,d}$ to the

general wall heat transfer coefficient.

$$h_{w,d} = 0.025\ (RePr)^{0.8}\ k_l/D_h \qquad (2.2j)$$

This formula is not well supported by experiments but has been incorporated primarily for parametric use. It is similar to the expression proposed in /14/.

Finally, the critical heat flux correlation used in SANDCMOT is empirical and due to Costa et.al. /15/

$$\phi_{crit} = 0.016\ \lambda\ G_z\ (1-x)\ Re_v^{-.25} \qquad (2.2k)$$

λ means the latent heat of vaporization, G_z the axial component of the mass flux vector Γ.

Additional modifications may be necessary when the cladding has molten and eventually has disappeared. Then, also radiative heat transfer between pins becomes essential. This case is included in SANDCMOT as described in /1/ but currently not operational.

The heat source term Q_w is obtained by integration of the heat flux ϕ over all pin or structure surfaces. In finite difference notation it is

$$Q_w = \Sigma_w\ A_w/V\ \phi_w$$

where the index w denotes all particular solid surfaces adjacent to the fluid volume V.

2.4 Fluid heat flux

The fluid heat flux q has been taken into account primarily in order to describe interchannel heat mixing by heat conduction. This mixing effect might be important if strong temperature gradients exist or if the convection effect is small. Also, if by helical spacer wires thermal mixing is promoted this effect might be represented approximately by enhanced radial heat conduction. q is defined by

$$q = - k_f \nabla T_f = - k_f/c_{pf} \nabla h_f \qquad (2.21)$$

Here, the index f refers to fluid properties that in single phase flow are those of the very phase but in two phase flow have to be constructed by an appropriate average of properties of the two phases. In the latter case it is defined

$$h_f = x h_v + (1-x) h_l$$

$$k_f = \alpha k_v + (1-\alpha) k_l$$

$$c_{pf} = x c_{pv} + (1-x) c_{pl}$$

A formulation of q involving h_f is necessary if the methods developed by Patankar /20/ for convection/ diffusion problems are to be applied.

III. Numerical solution method

The conservation equations for mass, momentum and enthalpy, the various equations of state and the constitutive relations represent a complete two-phase flow model. Due to its complexity a numerical solution must be sought. This solution is to be obtained within a certain spatial domain which in our case is fixed by the pin bundle structure. Therefore, the model geometry chosen to represent a n-pin bundle will be discussed first.

III.1 Geometry

The basic idea to model a symmetrical n-pin bundle is to use a suitable cylindrical annular geometry. This way of representation has been discussed already in some detail in ref. /1/. Here, a brief summary will be given only. To explain the procedure the case of a seven pin bundle contained within a quartz tube will be considered. It is sketched in Fig. 1 together with the corresponding annular geometry.

In both geometries, the central pins are identical. The outer row of six pins is represented by a layer of annular rings. In successive order there is cladding material, the gap, fuel material, another gap and once more cladding. The coolant channels are also modelled by annular rings. They are defined in the original geometry by a circle drawn around the center pin with radius equal to the pitch. The radii of the model annular rings are determined in a way as to conserve the mass portions of the various materials to be represented. These mass based radii, however, have to be corrected whenever they are used to calculate an exchange area for heat or momentum transfer. To this purpose a set of correction factors is supplied that accounts for the volume to surface corrections. In Fig.1 also radial cross flow channels are indicated. Their geometry (e.g. cross flow area, hydraulic diameter and channel length) additionally has to be specified by input and is thought to be superposed onto the massive rings of solid material. The cross flow channels allow a treatment of two dimensional effects, like flow around a blockage, or incoherency

among several channels etc..

As the mass portions and exchange areas are preserved in the model geometry reasonable average values for the various flow parameters as well as for temperatures, friction forces and hydraulic diameters will be calculated. This is indeed confirmed by experience.

Within the coolant channels flow obstructions due to grid spacers or any other objects can be modelled by input. It is possible to define a small massive annular ring within a coolant channel that will cause a reduced hydraulic diameter and additional friction. Also, its thermal effects are taken into account. These flow obstructions can be different at various axial locations.

The geometric design is completed by the definition of a computational grid that serves to locate the various quantities. As a rule, velocities and derived quantities are defined at grid cell boundaries whereas all the other quantities are defined at the cell center, like pressure, density, void fraction, temperature, and enthalpy. This is indicated in Fig. 2. This choice also means that the control volumina for mass and enthalpy are shifted to those of momentum by half a mesh width. Both grids are staggered to each other.

Whenever variables are used at locations different from the ones by definition a simple average value is calculated. For example, at the northern cell interface (the cell boundaries will symbolically be denoted by north, south, west and east) a center based quantity F usually is calculated via

$$F_{j+1/2} = (DZ_j F_j + DZ_{j+1} F_{j+1})/(DZ_j + DZ_{j+1}) \qquad (3.1a)$$

where DZ is the axial mesh spacing and j the axial node index. Radial averaging is currently modelled by simple avarages without any area weighting.

An exception to the above rule is the special averaging procedure of the void fraction in front of axial pressure gradients. According to suggestions of Wider and Tentner /18/ one should use (upward flow is assumed) :

for flow contractions ($\alpha_{j+1} < \alpha_j$)

$$\alpha_{j+1/2} = 1.67\ \alpha_{j+1}\ \alpha_j\ /(\alpha_{j+1} + \alpha_j) \qquad (3.1b)$$

for flow expansions ($\alpha_{j+1} > \alpha_j$)

$$\alpha_{j+1/2} = \alpha_{j+1}$$

If these expressions are chosen better pressure drop results are obtained at flow area changes than by simply averaging. Similar formulas were also obtained by Schmuck /19/ who used a factor 2.o instead of 1.67. His choice is adopted in SANDCMOT.

III.2 Solution strategy

In this chapter the major steps to obtain the desired solution of the two-phase flow problem will be summarized. After having defined the computational grid the differential equations describing mass, momentum and enthalpy conservation are transformed to finite difference equations by integration over a given control volume and forward time differencing of the inertial terms. Once the difference equations were established the major integration steps are as follows:

1. Mass and momentum equations are combined to obtain a Poisson equation for the pressure distribution. In case of two-phase flow also the enthalpy equation is required in order to express the density increment, in particular the void fraction change due to energy deposition and convection.
2. Once the new pressure distribution is known the momentum equations are solved for the advanced time velocities.
3. The updated velocities are used to calculate new mass density and enthalpy distributions.
4. Finally, advanced values of void fractions, vapor qualities and of some other derived quantities like flow rates, slip ratios etc. are calculated. This step completes one computational cycle.

The solution procedure outlined above essentially is as in the original SANDCMOT version /1/. However, due to the two-phase nature of the flow some distinct differences do exist. The most important one may be that different to the case of single phase flow the energy equation has to be coupled to the pressure equation. This necessity arises because the density increment $d\rho$ will depend on dp and $d\alpha$ in a two-phase situation :

$$d\rho(p,\alpha) = \alpha d\rho_v + (1-\alpha)d\rho_l + (\rho_v-\rho_l)d\alpha \qquad (3.2a)$$

All the density increments can be expressed by dp because of the assumed saturated conditions. For example, if ρ_v is known as a function of the saturation temperature TSAT its differential can be written as follows

$$d\rho_v = d\rho_v(TSAT)/dTSAT\ (dTSAT(p)/dp)\ dp$$

The same is true for $d\rho_l$. In order to express the void fraction increment $d\alpha$, the enthalpy equation is inquired. Using the definition of ρh one has

$$d\alpha = (d\rho h - \alpha d(\rho_v h_v) - (1-\alpha)d(\rho_l h_l)) \,/\, (\rho_v h_v - \rho_l h_l) \qquad (3.2b)$$

Again, the $d\rho$'s and dh's of either phase can be expressed solely by dp. But $d\rho h$ has to follow from the energy equation. It is by this term that the information contained within the energy equation appears within the pressure solution. If $d\alpha$ is inserted into (3.2a) and the differentials are expanded as indicated above one may find

$$d\rho = R_p\ dp + R_h\ d\rho h \qquad (3.2c)$$

$$R_h = (\rho_v-\rho_l)/(\rho_v h_v - \rho_l h_l)$$

$$R_p = (\alpha d\rho_v/dTSAT + (1-\alpha)d\rho_l/dTSAT$$

$$- R_h \, (\alpha d(\rho_v h_v)/dTSAT + (1-\alpha) d(\rho_l h_l)/dTSAT)) \; dTSAT/dp$$

On the other hand, for a single phase situation the density increment can be expressed by help of the equation of state. If ρ is taken to depend on pressure and temperature its differential may be written as

$$d\rho(p,T) = (\delta\rho/\delta p) \; dp + (\delta\rho/\delta T) \; dT \qquad (3.2d)$$

where the first derivative is the inverse square of the thermal sound speed. Often, the second summand is small and can be neglected. Then the pressure and energy equation decouple and one has the form used in the original SANDCMOT version. In the actual version, the temperature influence is not totally ignored. The enthalpy equation is solved preliminarily with old time level velocities to obtain a good estimate of the advanced temperatures. Then, the temperature induced density change $d\rho = (\delta\rho/\delta T)dT$ is evaluated directly from $d\rho = \rho(T^{n+1},p^n) - \rho(T^n,p^n)$. It should be mentioned further that the single phase vapor situation is described by an ideal gas law so that the above evaluation is not necessary. ρ^{n+1} simply is given by $p^{n+1}/(RT^{n+1})$ with R the specific gas constant and T^{n+1} the estimated advanced vapor temperature.

III.3 Discretization

After the presented basic reasonings some more technical aspects will be described in order to explain steps 1-4 in some detail. The finite difference form of the three conservation equations may be stated as follows :

$$V d\rho/dt_{kj} + \Sigma_b \; n_b A_b G_b^{n+1} = 0 \qquad (3.3a)$$

$$G_b^{n+1} = a_b + n_b d_b \Delta p_b^{n+1} \qquad (3.3b)$$

$$V d\rho h/dt_{kj} + \Sigma_b \; n_b A_b \; (G_b^{n+1} \; \langle h_f \rangle_b^{n+1} + q_b^{n+1}) =$$

$$Q_w + V(dp/dt_{kj} + \Sigma_b \; n_b W_b \Delta p_b) \qquad (3.3c)$$

The symbol d usually indicates a finite difference of some quantity with respect to time, for example

$$d\rho = \rho^{n+1} - \rho^{n} , \quad dt = t^{n+1} - t^{n} ,$$

where t is the time coordinate and n, n+1 denote the old and advanced time level. If the time index is omitted the old time level n is always implied. Furthermore, V is the volume of the computational cell centered around the midpoint with indices k,j. Here, k is the radial index and specifies the channel whereas j is the axial index. In addition, b is a short hand notion to specify the various boundary faces of cell k,j and n_b is a variable that only takes the values 1 and -1 depending on which boundary face is considered :

$$\begin{array}{lcccc} b: = & (k,j-1/2), & (k,j+1/2), & (k-1/2,j), & (k+1/2,j) \\ n_b = & -1, & 1, & -1, & 1. \end{array}$$

Also, by the index b either the radial or axial component of the mass flux density vector Γ is implied, in general the radial component for k+(-)1/2, the axial one for j+(-)1/2. Next, the symbol Σ_b means a summation over all surfaces b, and A_b denotes the area. Similar, Δp_B is a pressure difference across the corresponding boundary surface b. Note that pressures are always located at cell centers so that

$$\Delta p_b = p_{kj} - p_B$$

$$B: = (k,j+1), (k,j-1), (k-1,j), (k+1,j)$$

The duplets may sometimes also be referred to as north, south, west and east. Furthermore, the coefficients a_b and d_b appearing in the momentum equations contain explicit and implicit contributions of the various forces and are given in Appendix A.

The symbol $\langle F \rangle_b$, $F = h_f$, appearing in the enthalpy equation indicates a donor cell prescription. This means that the quantity F has always to be taken from the donor cell in dependence of the flow direction.

For example, if $G_{k,j+1/2}$ is positive, $\langle F \rangle_b$ equals $F_{k,j}$. If $G_{k,j+1/2}$ is negative, $\langle F \rangle_b$ acquires the value of $F_{k,j+1}$. This donor cell formulation is physically reasonable and gives bounded solutions. The numerical diffusion though is relatively high.

The velocity W used in the enthalpy equation denotes a mixture velocity and equals $\alpha W_v + (1-\alpha) W_l$. Although the two terms representing the pressure work are included in all formulas of this report and also are programmed they are suppressed in the actual calculation of the enthalpy distribution. The reason for this measure are stability problems that were occasionally encountered. Usually, the pressure work term is expected to be small. In the convective terms the vapor quality x was introduced in order to express the vapor and liquid flow rate in terms of G. This is possible because the slip ratio is equal in both radial and axial direction. Finally, it should also be mentioned that the same symbols were used to denote averaged or smeared quantities as well as the microscopic ones. In general this should not lead to any confusion because added indices always indicate the finite difference form.

If eqs.(3.3b) and the expressions for the density increments (3.2c,d) are substituted into eq. (3.3a) an equation for the pressure distribution is obtained. It has the general form

$$\beta_C \, p_C = \Sigma_B \, \beta_B \, p_B + \Pi \qquad (3.3e)$$

The various coefficients β and Π are given in Appendix B. As the pressure at central node C = (k,j) is related to all the other pressures in adjacent cells (this is indicated by the summation over index B) eq. (3.3e) is called a 5-point equation for the pressure. It can be solved by standard iterative procedures like line by line iteration, eventually combined with a relaxation technique /20/. A somewhat modified form is used in SANDCMOT, however. It is observed that the axial part of eq.(3.3e) can easily be solved by Gaussian elimination provided the radial cross flow rates are known. These now are determined first from the radial momentum equation. In this equation the pressure terms appear at the advanced time level. Best estimates of these pressures are used and the solution finally is

found by iteration. If only two connected channels exist no iteration is necessary. Once the radial flow rates are known they are substituded back into the axial pressure equation which is solved for the final pressure distribution. This special way of obtaining the solution does not offer specific advantages but is simply due to convenience.

As the density increments involve the change in temperature or in case of two-phase flow the change of enthalpy $d\rho h$ the pressure matrix coefficients β contain the fluid enthalpy h_f at the advanced time level (see Appendix A). Therefore, in order to set up the pressure matrix the enthalpy equation has to be solved in a prior step. To accomplish this, it is assumed at this step that the slip ratio is one so that ρh equals ρh_f. As the fluid heat flux is also expressible in terms of h_f equation (3.3c) can be written solely in terms of h_f. The resulting equation describes the combined convection diffusion problem of fluid enthalpy h_f. For such problems the numerical methods developed by Patankar and Spalding (see /20/) are applicable. Starting from an exact solution of the one-dimensional problem the relative importance of convection and diffusion is taken into account by a certain function of the local Peclet number $P_e = (\rho u)_e (\Delta x)_e/\Gamma_e$. Here, e denotes a cell boundary location (in this example the east boundary) and Γ is the diffusion coefficient (in our case k_f/c_{pf}). This function also appears in the finite difference formulation. Following the notation of Patankar /20, p.94/ the one-dimensional steady state diffusion/convection problem leads to the following finite difference expression

$$a_P h_P = a_E h_E + a_W h_W$$

where the coefficients are given by

$$a_E = (\Gamma/\Delta x)_e A(|P_e|) + \max(-G_e, 0.)$$

$$a_W = (\Gamma/\Delta x)_w A(|P_w|) + \max(G_w, 0.)$$

$$a_P = a_E + a_W + (G_e - G_w) \qquad (3.3f)$$

$A(|P|)$ is chosen according to the so-called power law

$$A(|P|) = \mathrm{Max}(0.0,\ (1.-0.1|P|^{5}) \qquad (3.3g)$$

When eq. (3.3c) is assembled it has the desired 5-point form with similar coefficients as specified above and is solved by standard iterative procedures. It should be noted that during the precalculation step the mass flow rates are used at the old time level. Later when the new velocities were obtained eq. (3.3c) is solved again using the final flow rates.

As the advanced density ρ^{n+1} is needed in eq. (3.3c), also the mass equation (3.3a) is solved using old time level flow rates. However, different to the form stated in (3.3a) a donor cell prescription is used in the convective terms. This choice is preferred because of its superior stability characteristics. No inconsistency exists because eq. (3.3a) in the form stated is solely used to derive the pressure. The following finite difference equations are solved that again exhibit the desired 5-point form

$$V d\rho/dt_{kj} + \Sigma_b\ n_b A_b (G/\rho)_b^n\ <\rho^{n+1}>_b = 0 \qquad (3.3h)$$

Finally, the three steps leading to the pressure equation are summarized once more. First, an estimated new mass density distribution is calculated according to eq. (3.3h). Then, the enthalpy equation is solved in terms of h_f and using old time level mass flow rates. If one cell is in a single phase state, new estimated temperatures are derived and used to determine the thermal density change according to eqs. (3.2c,d). For two-phase cells the pressure matrix coefficients β contain the enthalpy increments. Finally, the pressure matrix is set up and eq. (3.3e) is solved. This completes step 1 and provides the new pressure distribution.

In step 2 the momentum equations are solved for the new mass flow rates using the new pressure distribution. Also, advanced velocities are determined based on densities from the precalculation step.

In step 3 the mass and enthalpy equations are solved again using updated mass flow rates. Finally, new void fractions and vapor

qualities are calculated in step 4. This is accomplished using both the mass density and fluid enthalpy h_f. One has

$$\alpha_1 = (\rho-\rho_l)/(\rho_v-\rho_l) \tag{3.3i}$$

$$x_2 = (h_f-h_l)/(h_v-h_l)$$

$$S = S(x_2,\rho_v,\rho_l)$$

$$\alpha_2 = x_2\rho_l/(x_2\rho_l + (1-x_2)\rho_v S),$$

As the void fractions α_1 and α_2 will differ slightly the true void fraction is determined by an harmonic average

$$\alpha = 2\ \alpha_1\alpha_2/(\alpha_1+\alpha_2) \tag{3.3j}$$

It has the property that whenever one of the factors is zero also α will be zero. If both α_i are equal, α will acquire the same value. From α, the vapor quality x is calculated according to eq. (2.1d). This step completes one computational cycle.

III.4 Comments

Some additional comments are in place. In order to solve the pressure, enthalpy and mass equations appropriate boundary conditions have to be specified. As the radial boundaries of the pin bundle are solid and no flow across them is possible only the conditions at the bundle inlet and exit are needed. These are the time dependent values of inlet pressure and temperature. In the actual version, only single phase flow at the boundaries is assumed. A two-phase version, e.g. two phase flow at the inlet and exit boundary, could be implemented in a future development if this appears necessary.

Boiling is initiated when the fluid bulk temperature exceeds the local saturation temperature by a user specified superheat. This superheat problem was investigated experimentally with the result that under

reactor accident conditions the initial liquid superheat will be neglegible /2/. Once the boiling criterion is fulfilled a vapor quality is defined according to

$$x = (h_f - h_l)/(h_v - h_l) \tag{3.4a}$$

where the phasic enthalpies are evaluated at the saturation temperature. The corresponding void fraction is found by eq.(2.1d) under the assumption of no initial slip (S=1).

The source term Q_w appearing in the energy equation of the coolant describes the heat being transferred from the fuel pins to the coolant. This quantity has to be evaluated prior to any solution of the fluid enthalpy equation. This is achieved by solving the radial heat conduction equation within the fuel pins and the coolant. Heat convection within the coolant is not taken into account in this step but later when the enthalpy equation is solved. This is an example of the so called fractional step method. The radial heat conduction equation in cylindrical coordinates reads

$$\rho c_p \delta T/\delta t + 1/r\ \delta/\delta r(rk\delta T/\delta r) = q' \tag{3.4b}$$

If this equation is intergrated over certain control volumina within the fuel rod and an implicit finite difference scheme is used a system of equations is obtained that can be cast into the following form (see for example ref. /1/)

$$C_{jr}\ T_r = \mathcal{T}_j \tag{3.4c}$$

C is a tridiagonal matrix whose elements are composed of the thermal inertia terms $V_j \rho c_p/dt$ of the various nodes and the heat transfer coefficients between adjacent nodes. T is a column vector containing the nodal temperatures of fuel, clad and coolant. $\mathcal{T}$ is a vector that contains the volumetric heat source terms q' and old time level quantities. If the coolant is in a single phase state, its thermal properties are those of the specific phase. If a two-phase situation is encountered, the coolant's effective heat capacity has to be

specified including possible evaporation or condensation effects. As the phase transitions tend to stabilize the temperature and thus the pressure, the heat capacity at constant pressure is used. From ref. /21/ the saturated liquid heat capacity is

$$C_{pl} = C_{SAT} + T\ \alpha_p\ DpdT/\rho_l$$

$$C_{SAT} = (dh_l/dT)_{sat} - DpdT/\rho_l$$

$$\alpha_p = \alpha_{SAT} + \beta_T\ DpdT$$

$$\alpha_{SAT} = -(d\rho_l/dT)_{SAT} / \rho_l\ , \qquad DpdT = dPSAT/dT$$

Generally, the thermal compressibility β_T is small and is neglected. Similarly, for the vapor phase one has

$$C_{pv} = C_{SAT} + T\ \alpha_p\ DpdT/\rho_v$$

$$C_{SAT} = (dh_v/dT)_{sat} - DpdT/\rho_v$$

$$\alpha_p = (\alpha_{SAT})_v / (1.-DpdT/\gamma_v)$$

$$\alpha_{SAT} = -(d\rho_v/dT)_{SAT} / \rho_v$$

$$\gamma_v = 0.46652 - 0.025165\ (T_c - T)^{1/2} + 3.4175E\text{-}4\ (T_c - T)$$

Now the coolant's effective heat capacity is

$$c_{p,tp} = (\alpha\rho_v C_{pv} + (1-\alpha)\rho_l C_{pl})/\rho \qquad (3.4d)$$

This value has been used in sample calculations and found to sometimes cause problems. A simple alternative is to use

$$c_{p,tp} = h_f/TSAT$$

in the radial heat conduction solution step giving also reasonable

results. The finite difference heat conduction equation (3.4c) can be solved by Gaussian elimination. As a result, the fuel rod surface temperature T_w as well as the coolant temperature T_{cool} are obtained. The heat flux ϕ and Q_w can now be calculated according to eqs.(2.2g, ff.).

The numerical solution procedure as outlined above can be characterized as being semi-implicit. An implicit treatment is attempted whenever the resulting algorithm does not become too involved. So, the pressure gradient terms are implicit removing the time limitations due to sonic wave propagation. However, parts of the wall friction force and of the convective terms in the momentum equations are explicit. Therefore, at least, a time step limitation due to mass convection is present. This one can become more and more restrictive as the vapor velocities do increase. Another restriction results from the demand that no more liquid can be vaporized than is present in a certain node. With these restrictions to the time step generally a stable solution is obtained. However, some precautions concerning the pressure solution are necessary. Especially in the liquid phase due to its incompressible character high pressure changes can result if slight differences in the mass flow rates exist. This may even cause the pressure to become negative. To prevent this, a minimum pressure is defined which is 1/10th of the ambient pressure. Also pressure spikes are prevented by limiting the maximum pressure to 100 bar. Although these measures are disturbant a reduction of the time step size probably will remove their need. However, a not too small time step in between 0.1-0.5 msec was attempted and generally possible. Future improvements could concentrate on this point.

IV. TREAT-R5 experiment

The TREAT-R5 experiment/2/ was selected to guide the code development and to serve as a realistic test. In this experiment, a seven pin bundle contained within an hexagonal flow tube was exposed to a loss-of-flow transient while the pins were heated at 29 kW/pin = 167 kW/kg. The R-series test apparatus and the cross section of the 7-pin test section are sketched in Fig.3. An axial view of the piping system and the location of the pin bundle are presented in Fig.4. A summary of measured data is displayed in Fig.5. All these figures are taken from ref./2/ where further and more detailed information can be found.

The seven pin bundle is represented by the annular geometry shown in Fig.1. The hexagonal flow tube is modelled as an annular ring whose inner diameter is given by the requirement that it should enclose the same area as the flow tube. The inert housing and the molybdenum tubing that are present in the experiment to serve as a thermal barrier are also modelled as successive annular rings. The model radii R1-RD of the various annuli are summarized below in Table 1 (radii in /mm/).

R1	R2	R3	R4	R5	R6	R7	R8	R9	RA
2.47	2.54	2.921	5.692	6.152	6.222	8.679	8.749	9.142	10.40

RB	RC	RD
10.91	13.72	15.24

Table 1 : Radii of annular geometry (see Fig.1)

Meaning :

0.-R1 : fuel portion of inner pin
R1-R2 : gap inner pin
R2-R3 : cladding of inner pin
R3-R4 : first, inner coolant channel
R4-R5 : cladding outer pin row (inner side)
R5-R6 : gap outer pin row
R6-R7 : fuel portion of outer pin row
R7-R8 : gap outer pin row

R8-R9 : cladding outer pin row (outer side)
R9-RA : second, outer coolant channel
RA-RB : flow tube
RB-RC : helium gas layer
RC-RD : molybdenum tube

These radii can also be found in the sample input for the TREAT-R5 experiment which is reproduced in Appendix E. There, also the surface correction factors are specified that correct the mass based radii whenever they are used for determination of exchange areas. A detailed input description can be found in the code user manual /22/.

The various spacer wires between the pins and at the tube wall are not included in the present anlysis. The code, though, has a possibility to represent grid spacers that could be used in a somewhat modified form to also account for the spacer wires used in the TREAT tests. This possibility was not elaborated further in this work but is left as an issue of future developments. The axial representation of the pin bundle is illustrated in Fig.6. At the bundle inlet and exit one additional node is added to account for the piping system that is connected to the supply and exit tanks where the pressure boundary conditions are specified. Only one node is available because the present model does not have a very elaborated model of the inlet and exit pipe strings. This has the consequence that without further measures the characteristic oscillatory motions of inlet and exit liquid slugs during boiling progression cannot be modelled well. However, if the pressure boundary conditions include an oscillatory part also the slugs will exhibit these oscillations. There are various pressure drops occuring along the inlet and exit pipe section due to friction and irreversible pressure losses at several nozzles. These pressure drops are comprised and located at the bundle inlet and exit. They are described by the formulas

$$\Delta p(\text{inlet}) = 1/2\rho f_{in}|v_{in}|v_{in} \qquad (4.a)$$

$$\Delta p(\text{exit}) = 1/2\rho f_{ex}|v_{ex}|v_{ex}$$

f_{in} and f_{ex} are throttling factors that are assumed to have the general dependence

$$f_{in} = 0.316\ Re_{in}^{-1/4}\ (l_{in}/d_p + fi_1) + fi_2/Re_{in} \qquad (4.b)$$

$$f_{ex} = 0.316\ Re_{ex}^{-1/4}\ (l_{ex}/d_p + fe_1) + fe_2/Re_{ex}$$

v_{in} and v_{ex} are the velocities within the inlet and exit pipe section, d_p is the hydraulic diameter of the pipe and Re_{in}, Re_{ex} are the respective Reynoldsnumbers. Further, l_{in} and l_{ex} are the lengths of the slugs in inlet and exit pipe sections. The friction factors fi_1, fe_1 essentially were adjusted to reproduce the stationary coolant flow rate during the early test phase before flow coast down using the measured bundle inlet pressure of 5.88 bar. The other two parameters were chosen to give a reasonable inlet pressure during the boiling period of order 1.6E5 Pa and a sufficiently rapid flow decay. As a result it was obtained

$$fi_1 = 5.0E6 \quad , \quad fe_1 = 5.1E6 \ ,$$
$$fi_2 = 1.0E4 \quad , \quad fe_2 = 4.0E4 \ .$$

To start a calculation, the geometry, inlet and exit temperatures as well as corresponding pressures, the reactor power, axial and radial power profiles along and within the pins, the coupling factors and the initial state conditions have to be specified by code input. These data generally are known from the experiment records or can be derived by reasonable assumptions. They are contained in the TREAT-R5 sample input reproduced in Appendix E. Major results of the recalculation to be compared to the experiment are the flow rates (Figs.7,8), the void volume variation (Fig.9) and the coolant temperatures (Fig.10) at selected locations.

Two cases were investigated that only differ in the time dependent inlet pressure boundary condition supplied by input. In case 1 the nominal value as reported in the experimental results is taken. In this case the inlet slug only poorly oscillates after flow reversal as can be seen in Fig. 7. This behavior was attributed to the single node

representation of the inlet slug that does not allow a detailed pressure determination at the bundle inlet. In order to test the model when such oscillations are enforced an inlet pressure boundary was chosen that includes a sinuslike oscillatory component. The frequency was chosen according to the measurement (two cycles per second) and the amplitude was set to 5.E4 Pa. Now, in this second case the inlet slug follows the pressure oscillations and exhibits upward and downward motion as can be seen in Fig. 8. These results compare favourably to the experiment. This shows that indeed reasonable results are obtained provided the dynamic pressure build-up in the liquid slugs is correctly taken into account. In Figs.7 and 8, the experimental curve as well as the calculated mass flow rate at the bundle exit are included. The measured exit flow rate is not shown as it is strongly disturbed by the plenum gas release from the fuel pins (about one second after boiling inception) and thus is not comparable to the calculated values.

Comparing the void volume propagation both cases show similar results. Here, the results of the second case are presented in Fig. 9. It can be seen that the lower boundary compares well but that the upper slug has not been removed far enough out of the bundle. This tendency is already realizable before experimentally the upper slug is pushed away by the gas release that is not modeled. An easy explanation cannot be offered but two possible reasons are to be mentioned. First, it may be that too much inertia for the upper slug is introduced (by input) or eventually, too low plenum temperatures are calculated. Although other comparative runs with slightly different input data show a better agreement the presented results are a hint that some future improvements have to consider this point. In total the calculated void boundaries are reasonable which is an important result for the subsequent clad motion calculations.

Next, the calculated temperatures are to be compared to experimental findings in Fig. 10. Twelve thermocouples within the core were present at various locations along the fissile zone. Here, only the temperature at the upper end of the fissile zone is to be compared. Two other calculated temperatures within the upper blanket are additionally displayed. There seem to be two major discrepancies in comparison to the experiment. One is that after the start of flow

coast down calculated temperatures lie higher. The second one is related to single phase vapor conditions (α = 1.). In this case the code assumes a rather low vapor heat capacity of order c_p = 1300. W/kgK. Consequently, the vapor temperatures rise quickly and essentially acquire the temperature of the surrounding cladding. This, however, can reach temperatures far beyond the local saturation temperatures. Although also in the experimental results local fast temperature rises are reported it cannot be deduced clearly how far up they eventually have increased. If the reported temperatures are taken as they stand they, in the average, appear close to the saturation temperature corresponding to a pressure of order 2.E5 Pa. A possible explanation of the first point may be that the thermocouples probably were installed close to the hexcan wall where they are likely to indicate somewhat lower temperatures. This would also be in agreement with the slower experimental temperature increase. The second point may be related to the possibility that there still could be some liquid droplets around the thermocouples especially if they are close to the wall. In this case they could indicate saturation conditions. The temperatures of Fig. 10 habe been plotted again using loacal saturation temperatures whenever a single phase vapor state is reached. This is shown in Fig. 10a and a much better agreement during the advanced boiling phase can be seen.

When the temporal occurrence of some key events is compared the following results are found

Event	TREAT-R5	SANDCMOT
1. Start of flow coast-down	7.95 s	7.95 s
2. Local boiling	12.5-13.5 s	13.75 s
3. Inlet flow reversal	14.56 s	14.40 s
3. Dry-out indication	14.8 s	15.01*s
4. Fuel-pin clad failure	15.7 s	-
5. Start of clad motion	16.6 s	16.82 s
6. Hexcan failure	17.85 s	-

* based on α = 0.99 void fraction

Table 2: Summary of some key events

One can see that the time points are fairly well met within about 0.2 s. This is an encouraging result.

Finally, some additional calculated data are displayed on Figs. 11-20. There, it can be seen that liquid and vapor velocities may differ drastically and that the latter ones may be as high as 150 m/s (sometimes even up to 200 m/s).

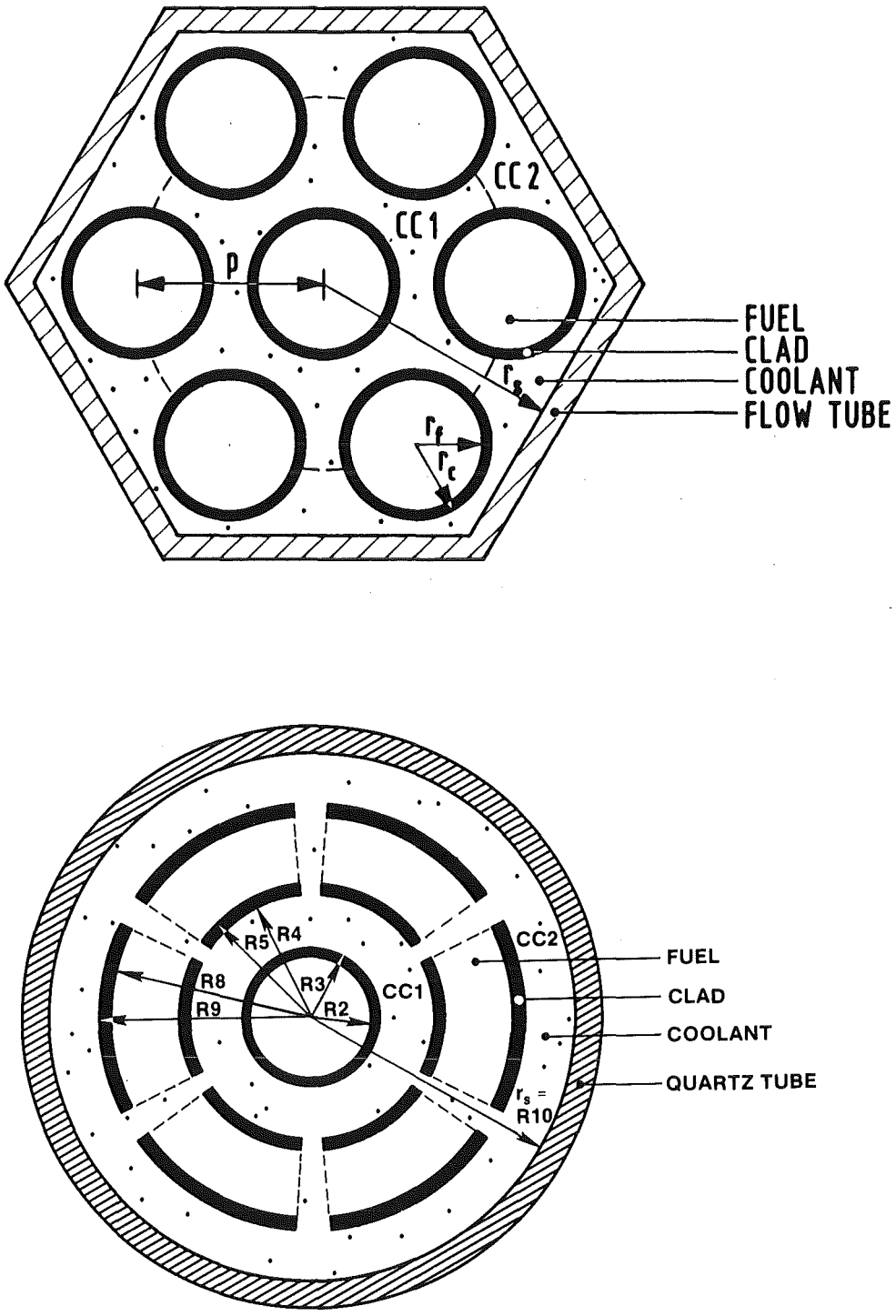

Fig. 1 : Seven pin bundle and model geometry

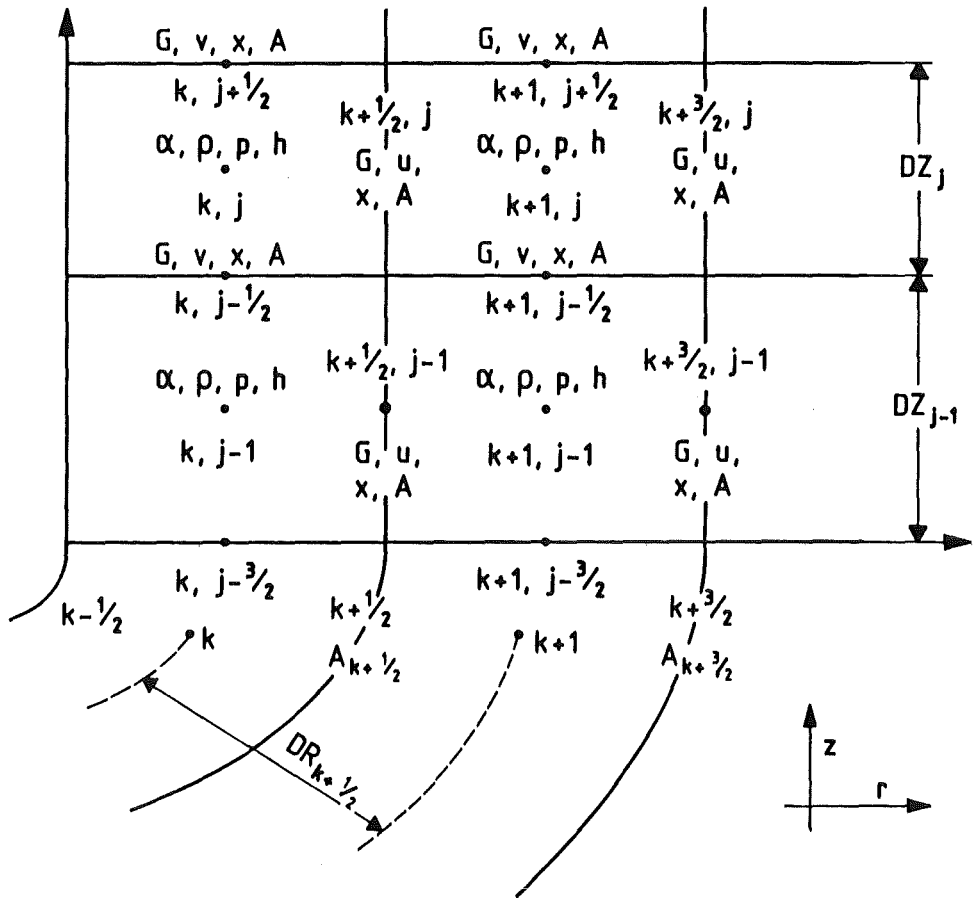

Fig. 2 : Computational grid layout

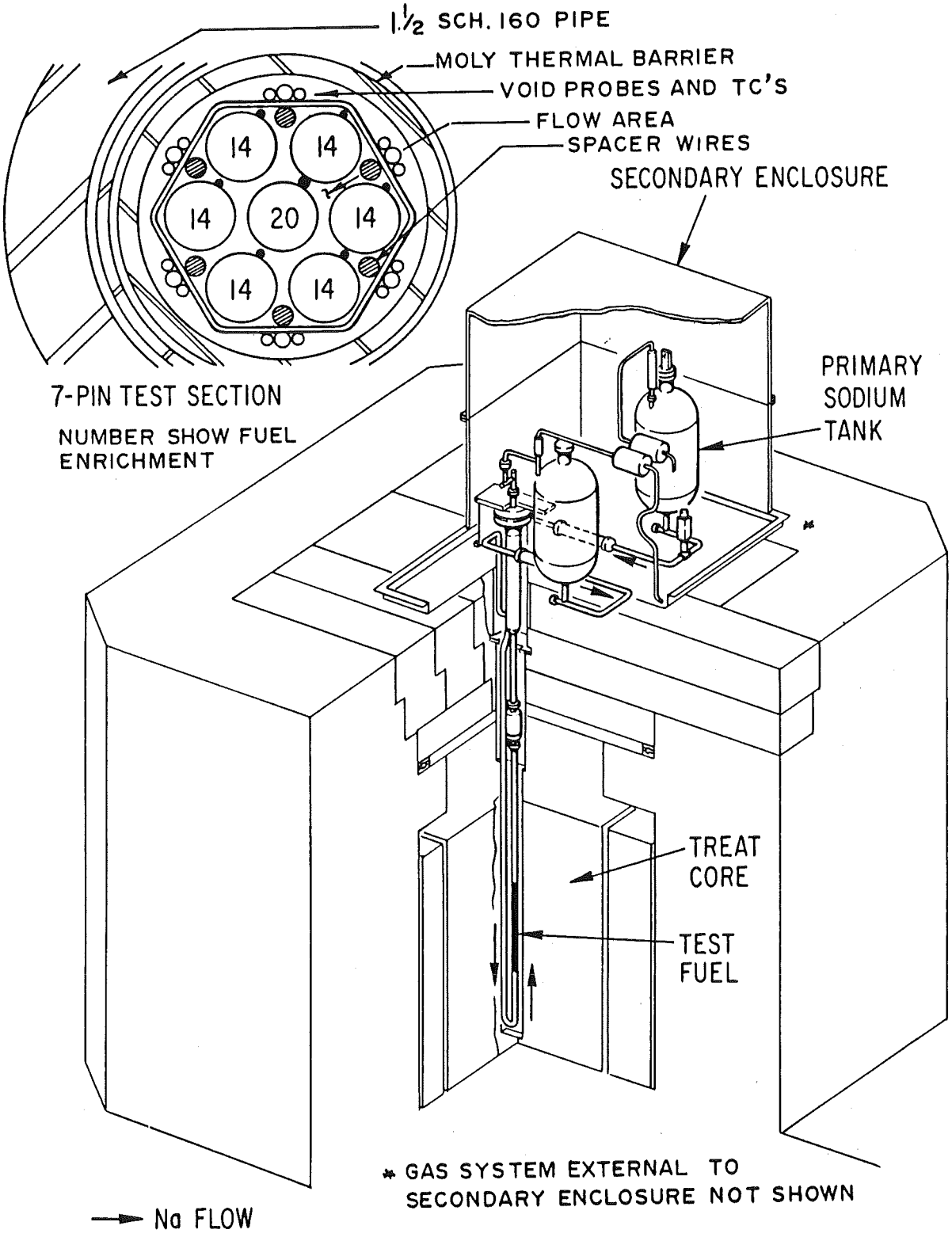

Fig. 3 : TREAT R-series test apparatus (reproduced from /2/)

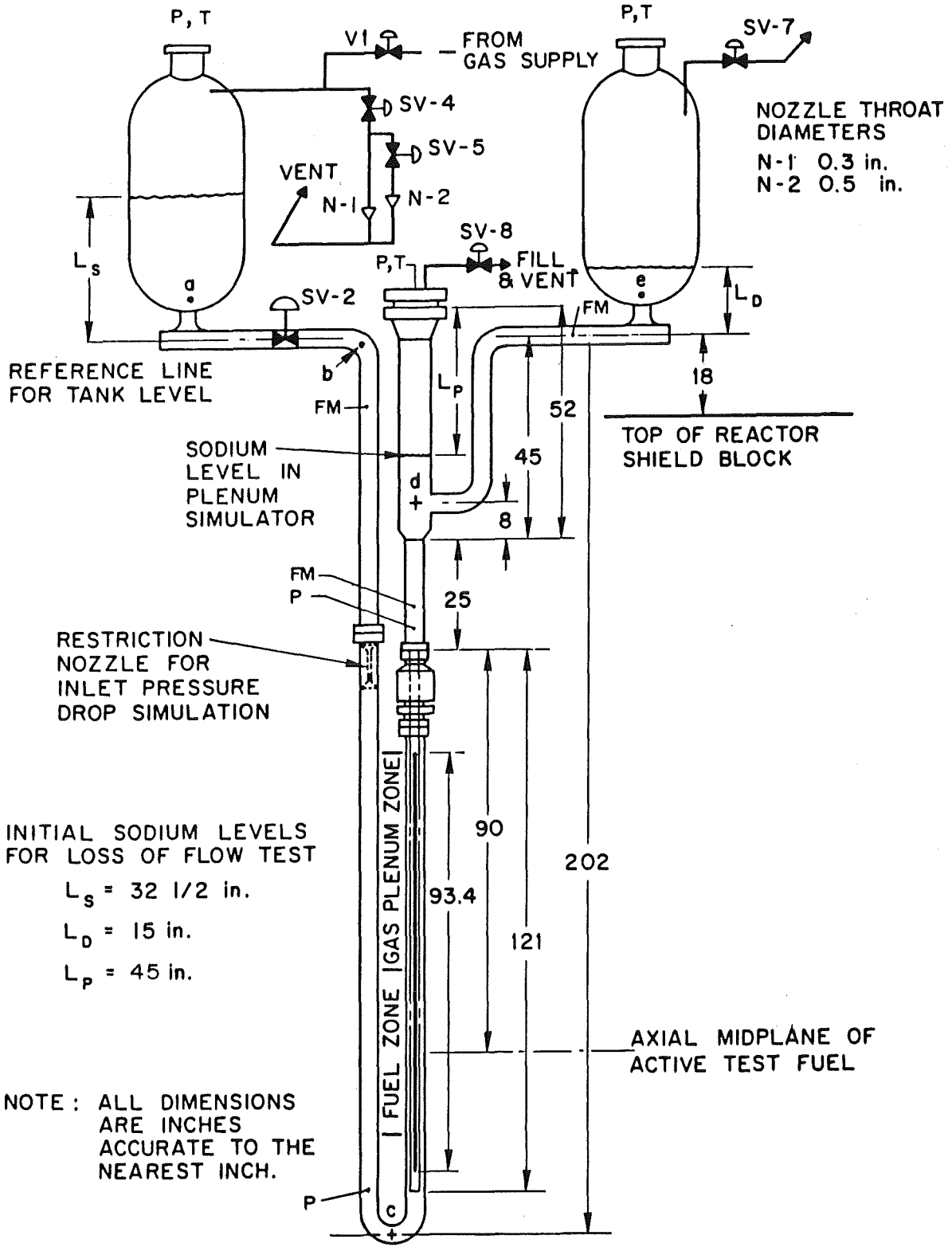

Fig. 4 : Axial view of test mock-up (reproduced from /2/)

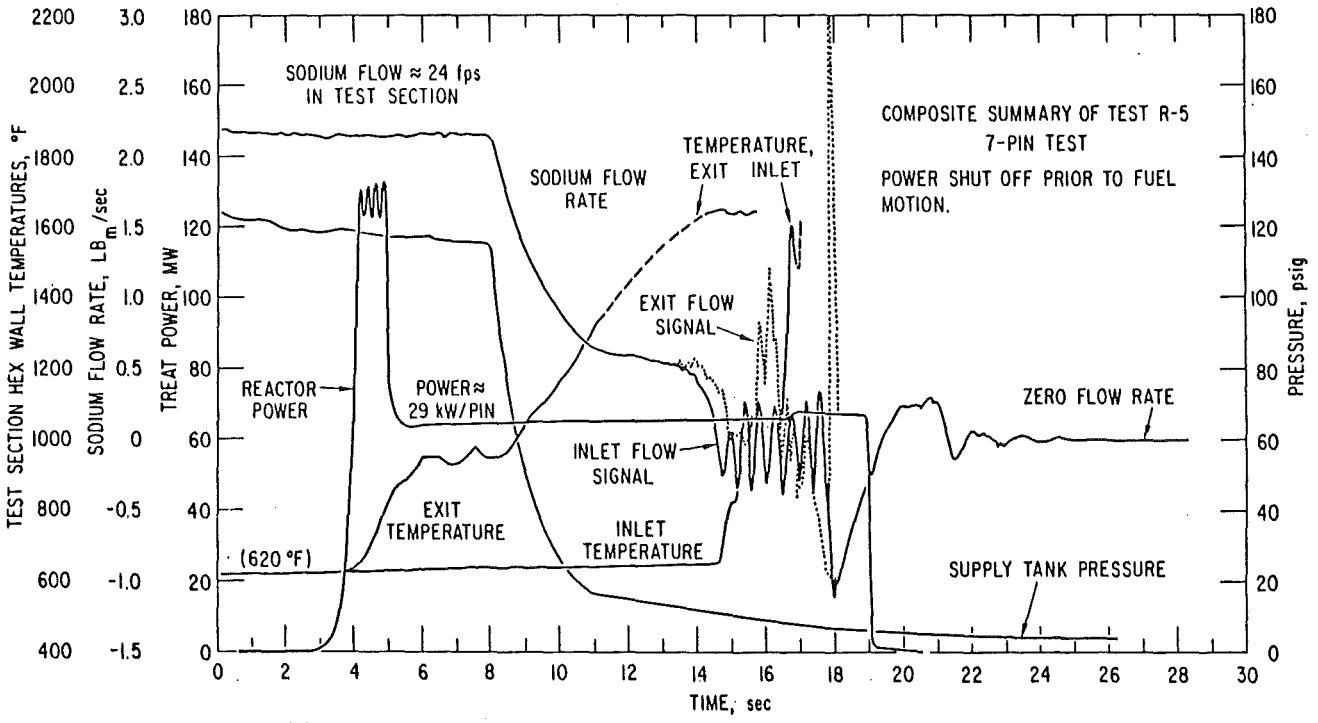

Fig. 5 : Summary of measured data (reproduced from /2/)

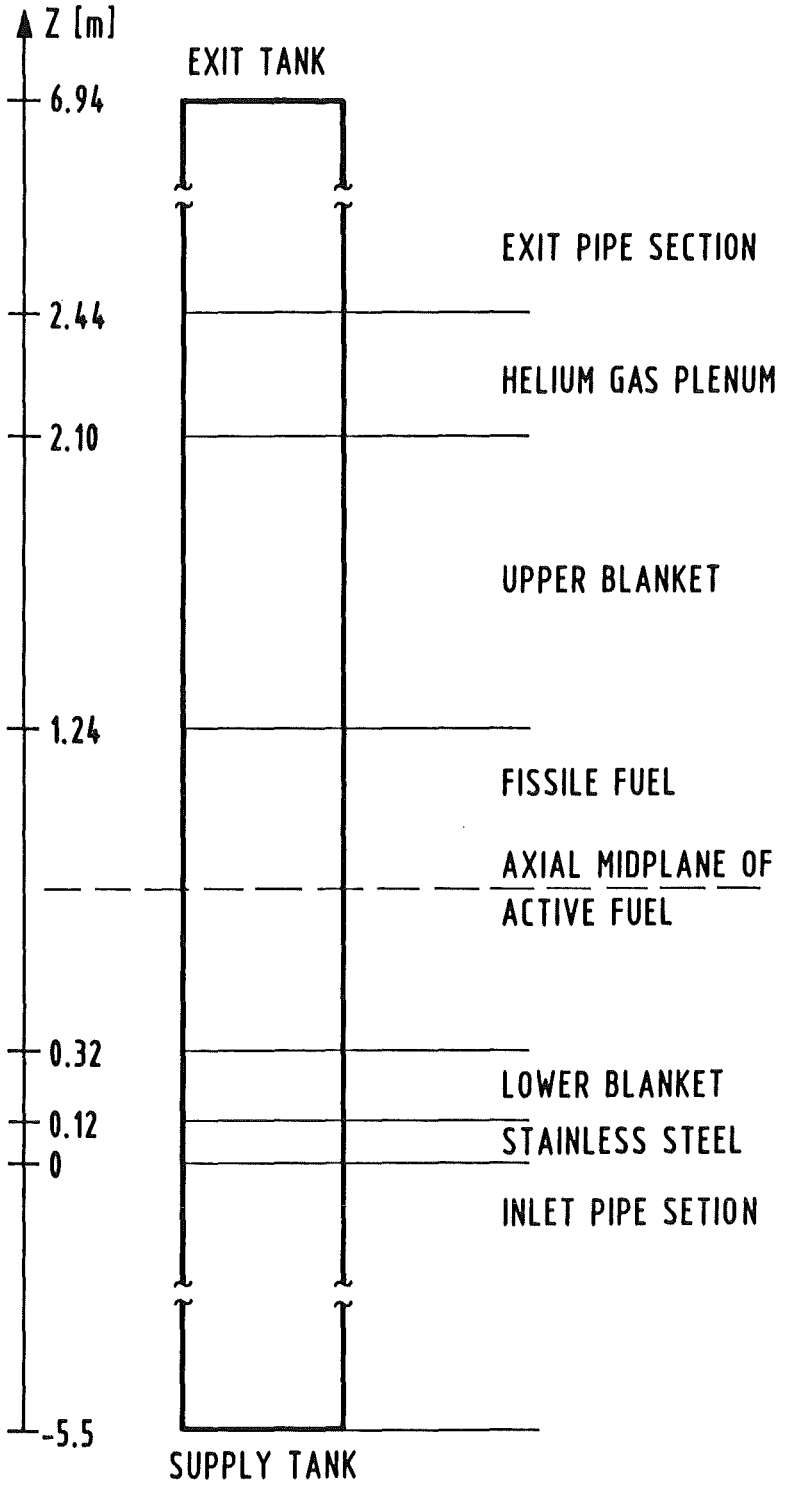

Fig. 6 : Axial representation of TREAT 7-pin bundle

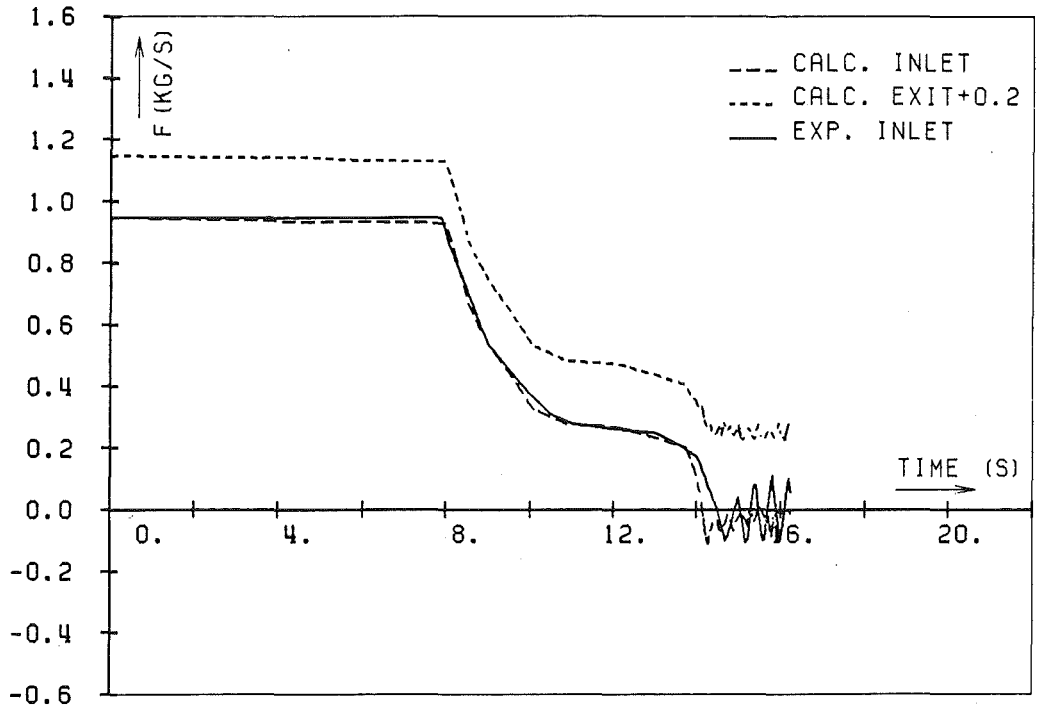

Fig. 7 : Calculated and measured flow rates, case 1

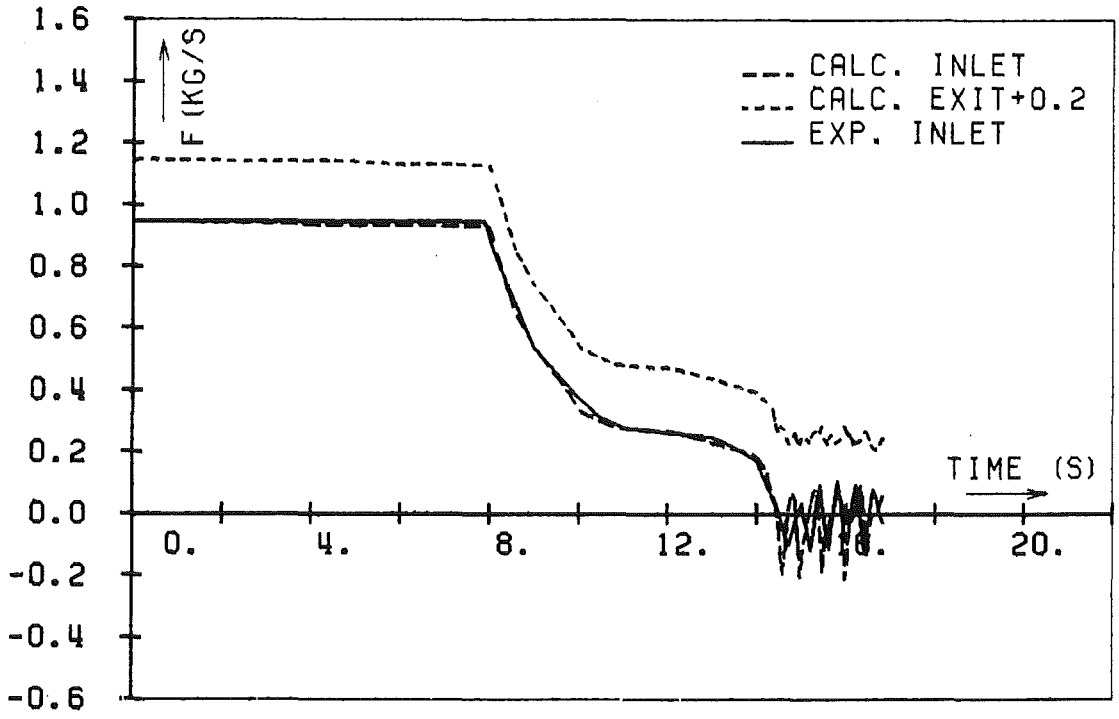

Fig. 8 : Calculated and measured flow rates, case 2

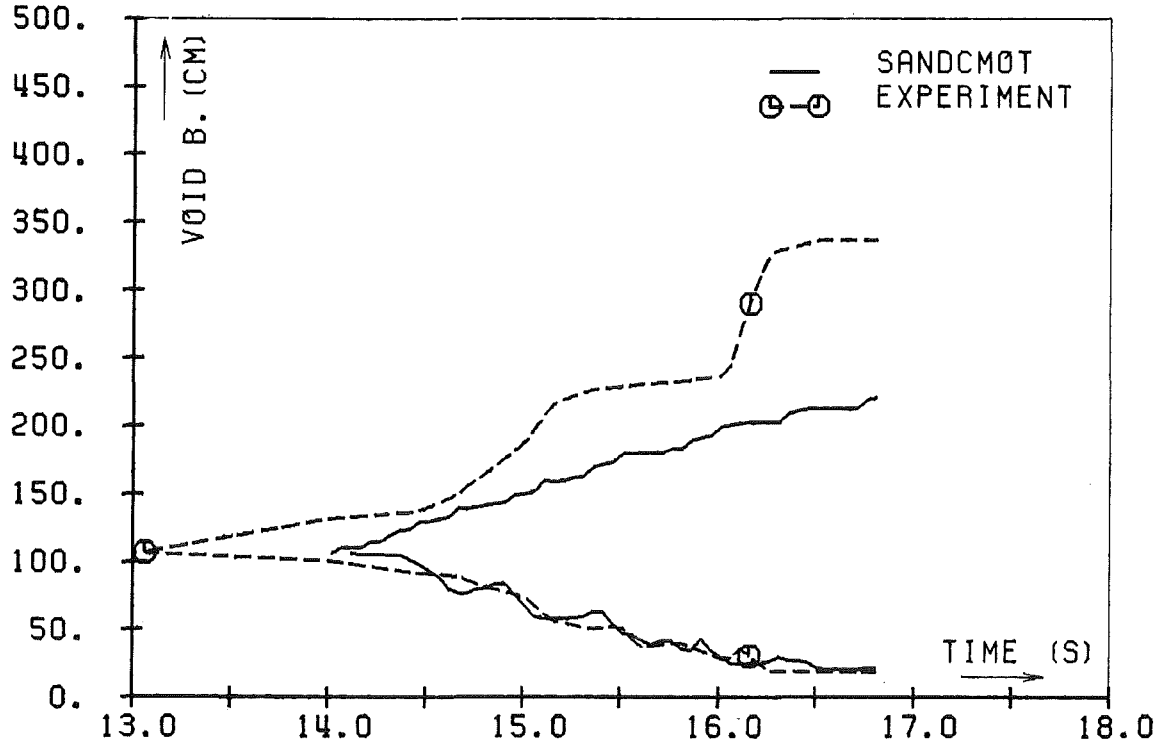

Fig. 9 : Calculated and measured void propagation

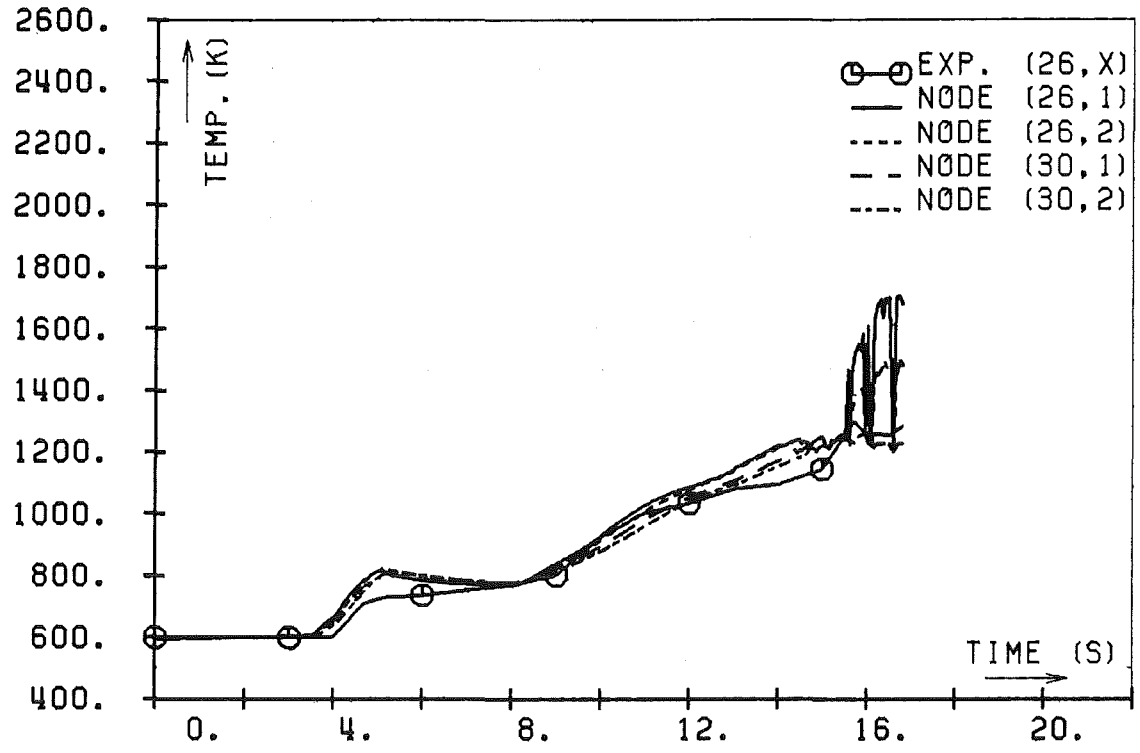

Fig. 10 : Calculated and measured temperatures

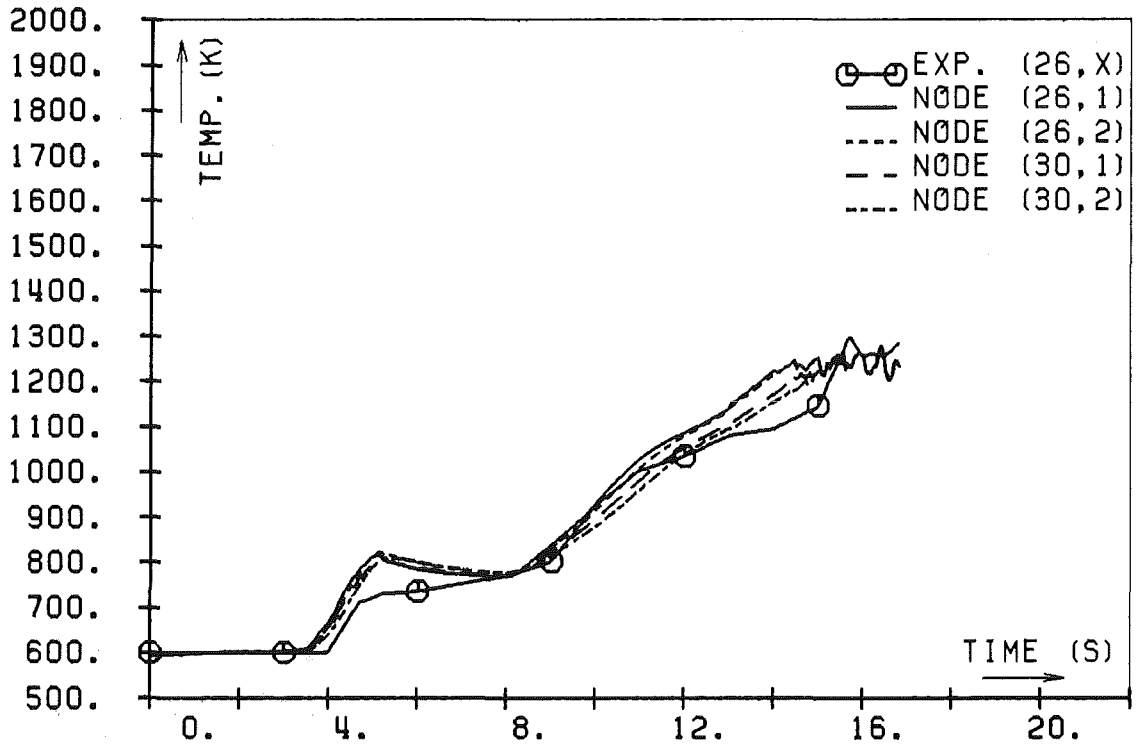

Fig. 10a : Calculated and measured temperatures (saturation conditions always) , X : thermocouples located at hexcan wall

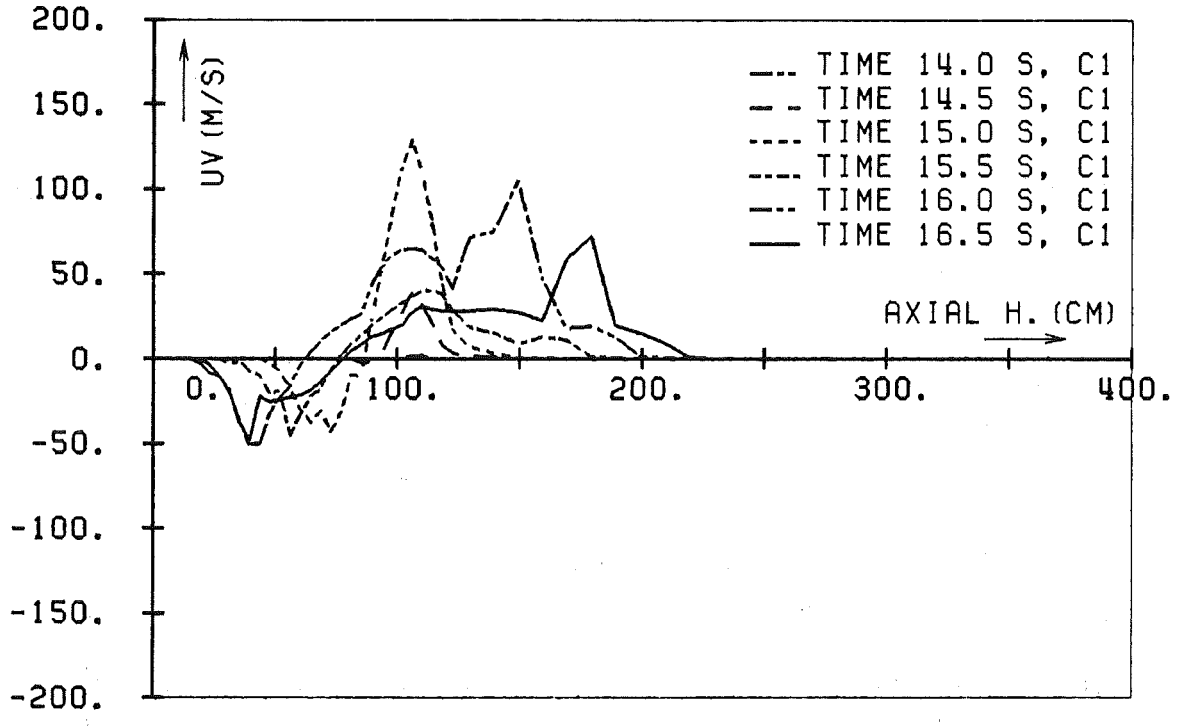

Fig. 11 : Vapor velocities, channel 1

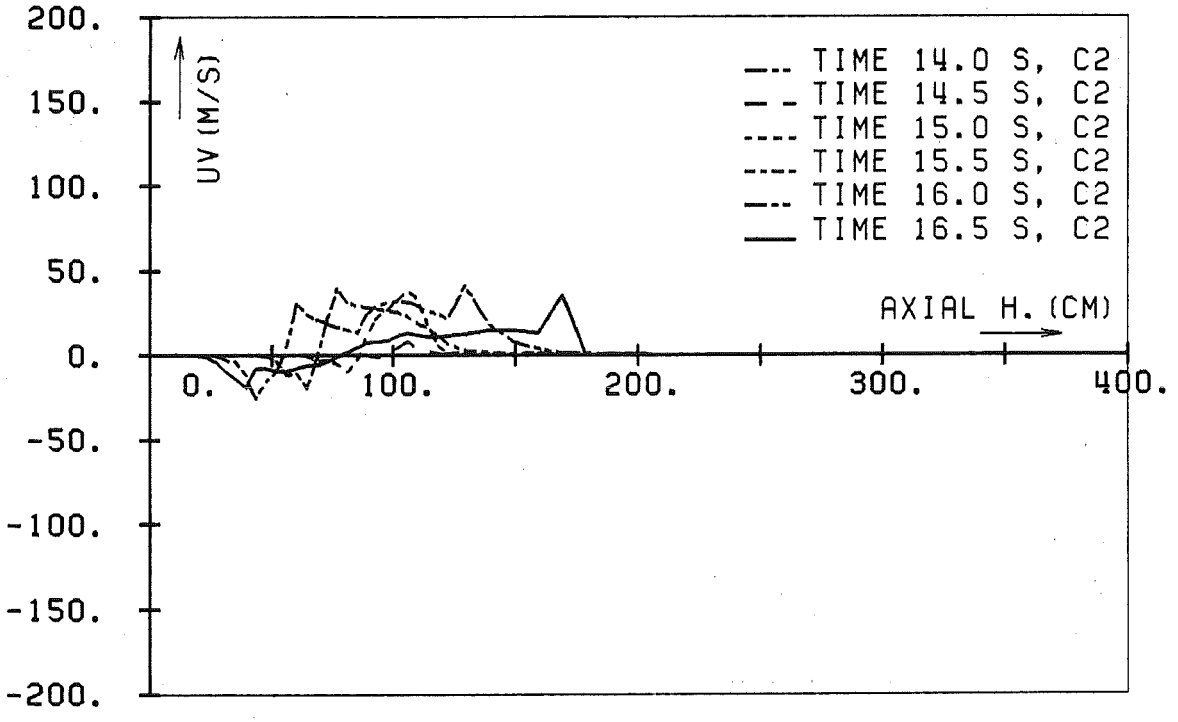

Fig. 12 : Vapor velocities, channel 2

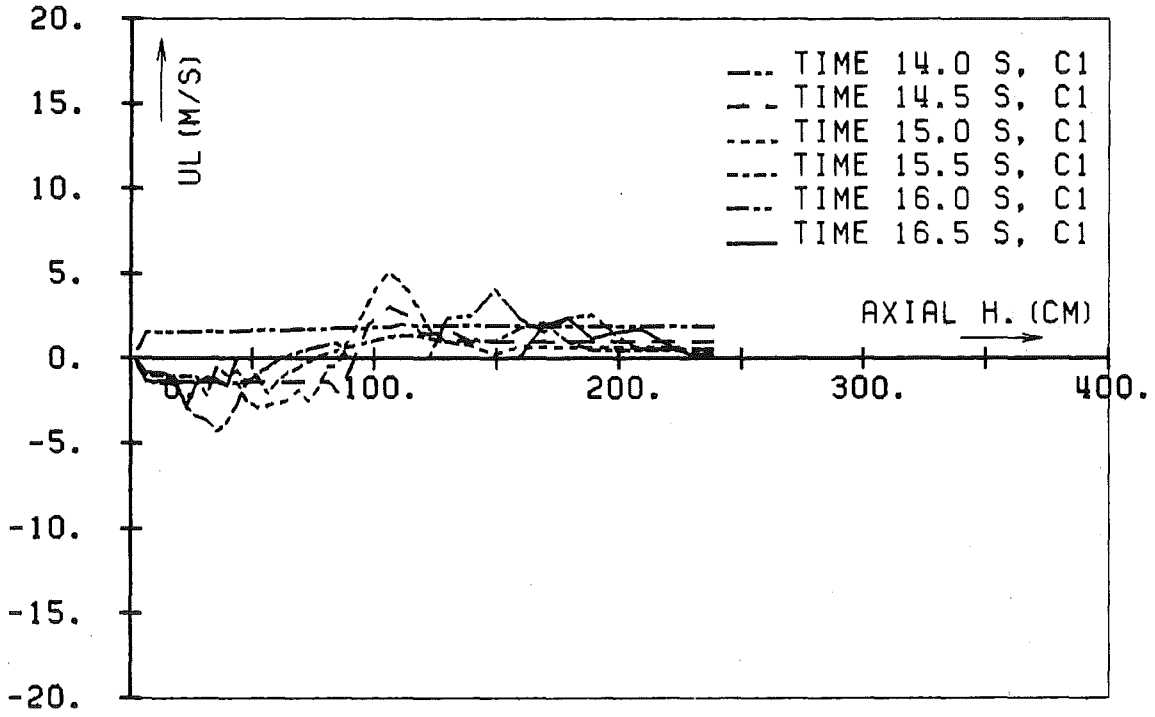

Fig. 13 : Liquid velocities, channel 1

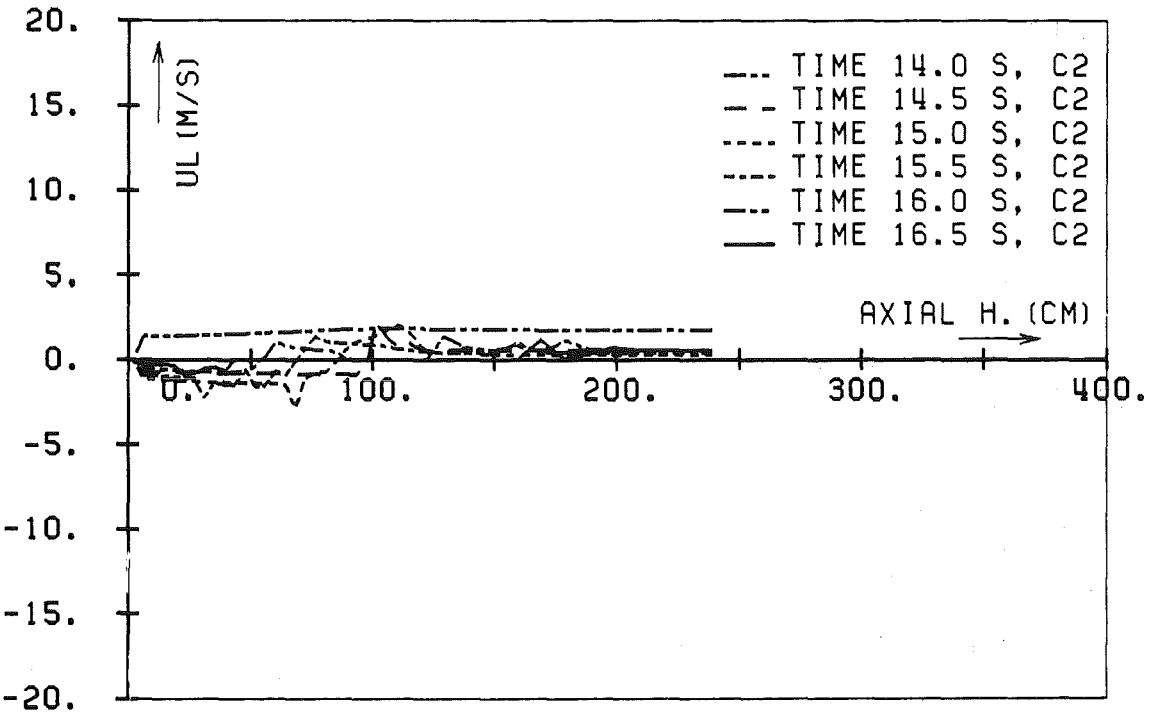

Fig. 14 : Liquid velocities, channel 2

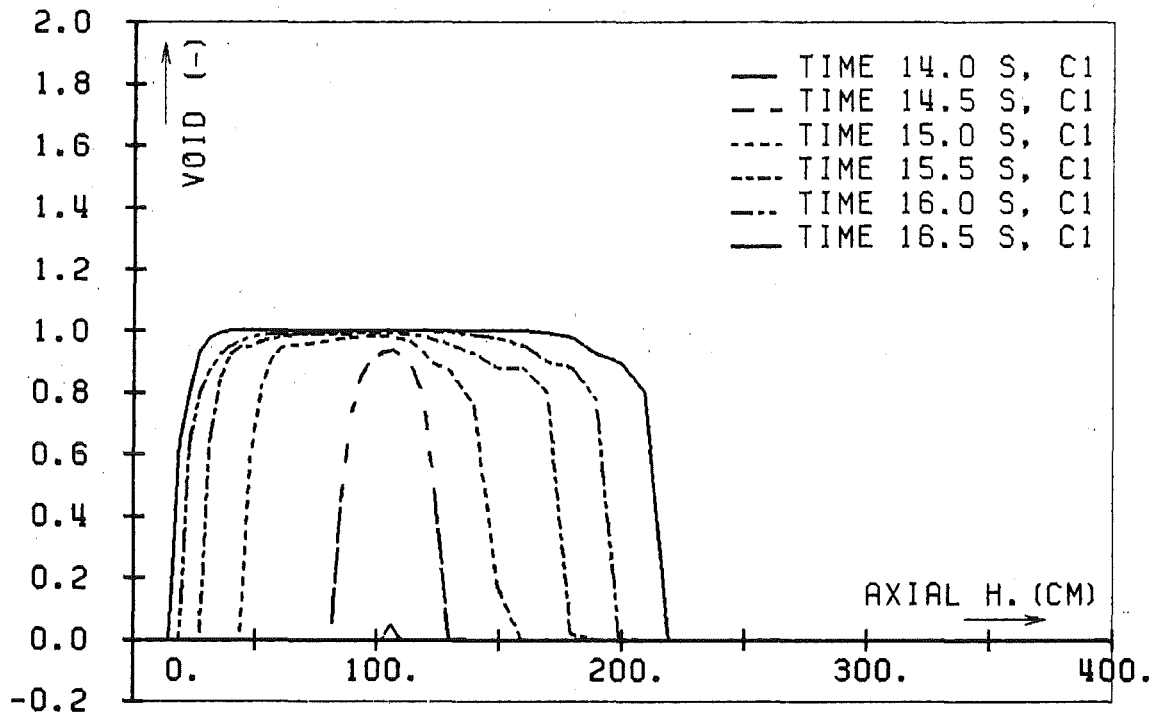

Fig. 15 : Axial void profile, channel 1

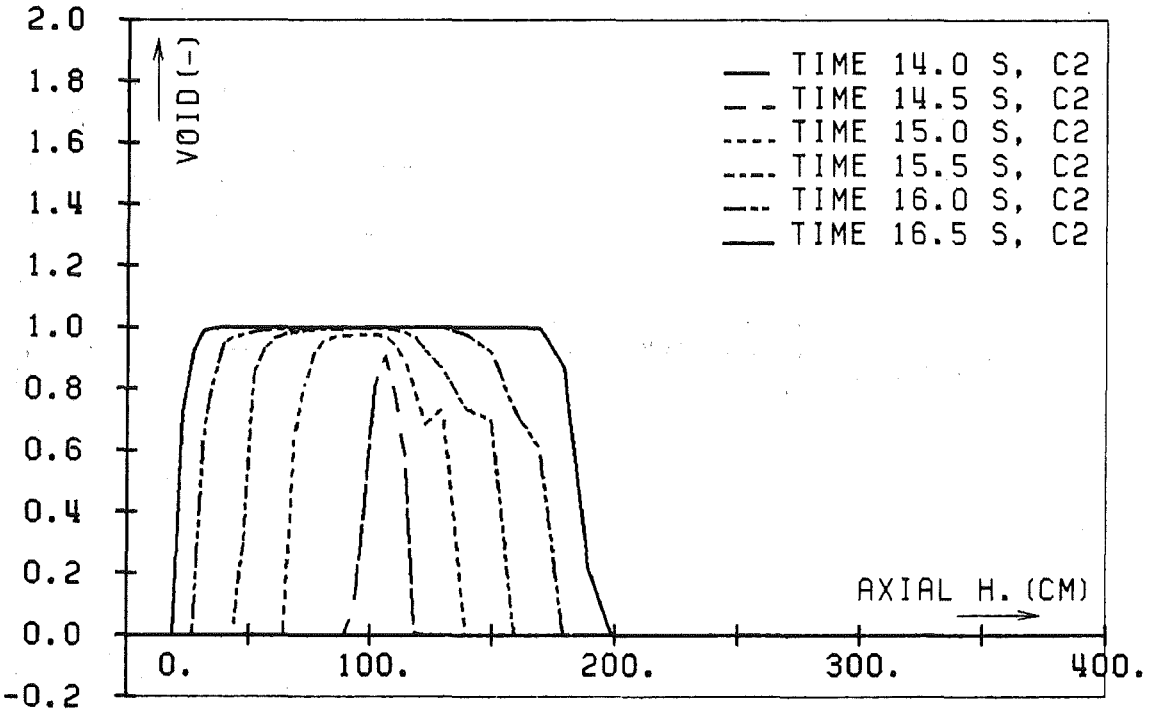

Fig. 16 : Axial void profile, channel 2

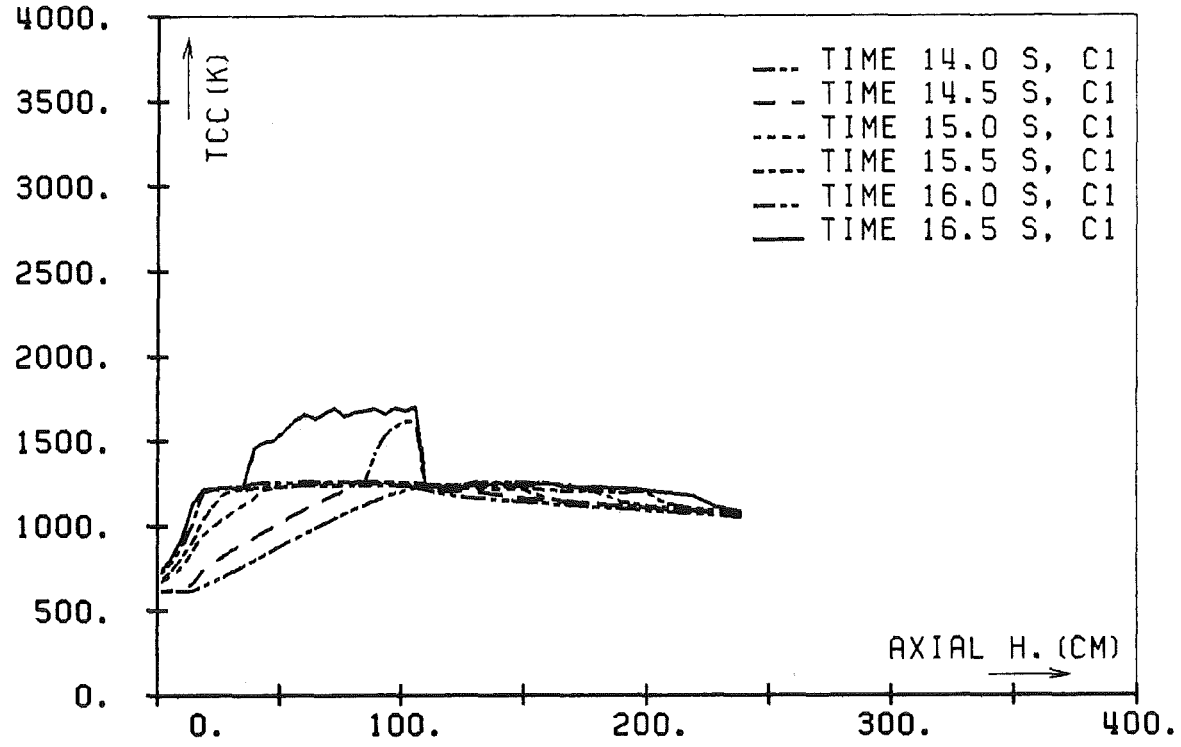

Fig. 17 : Axial temperature distribution, channel 1

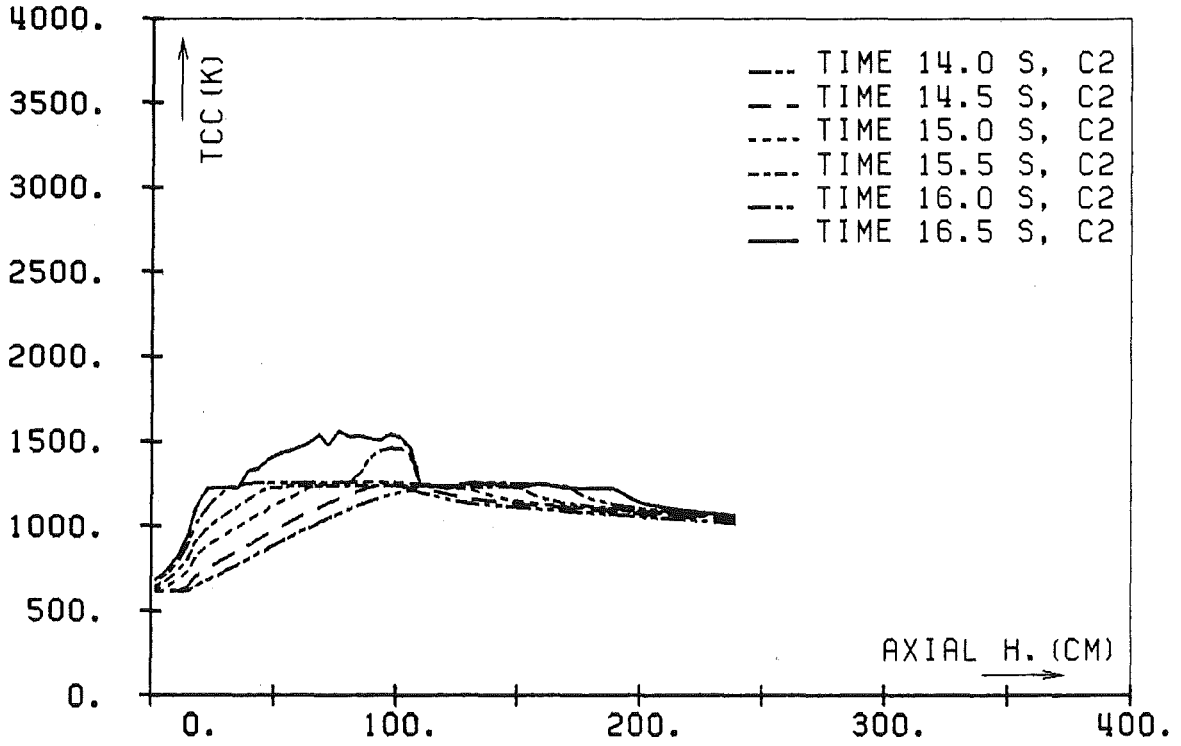

Fig. 18 : Axial temperature distribution, channel 2

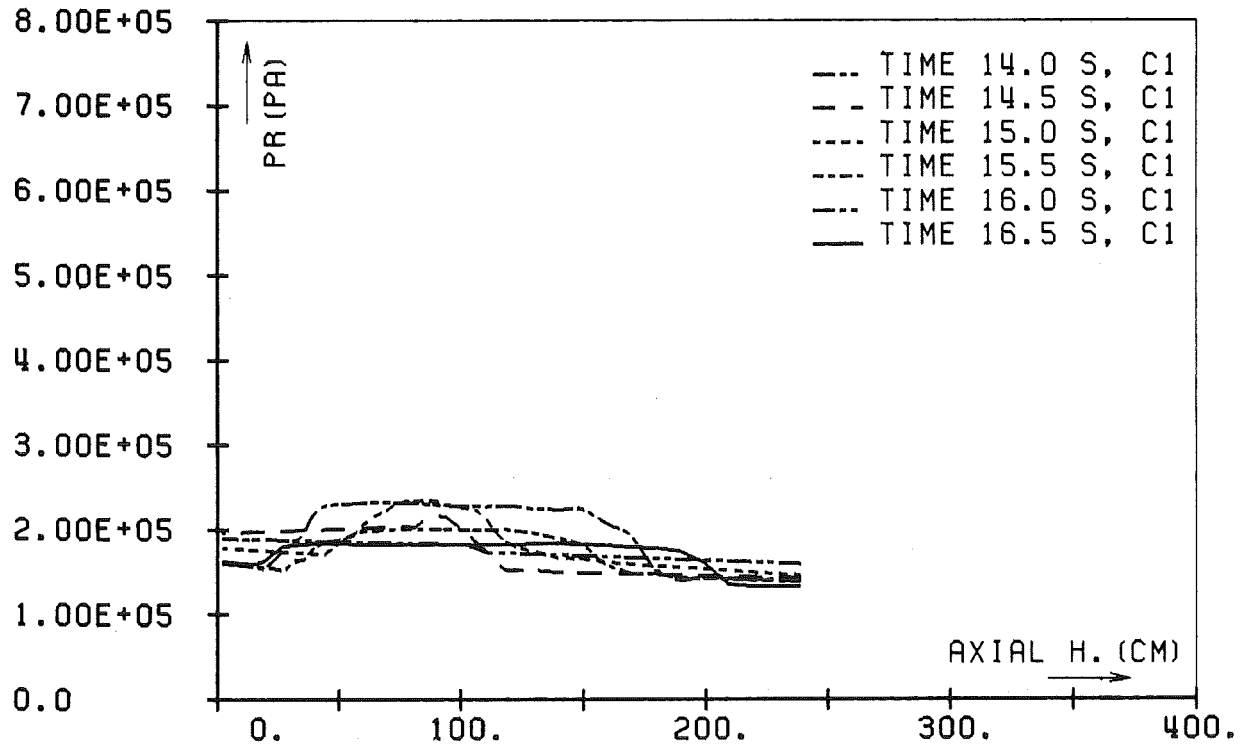

Fig. 19 : Axial pressure distribution, channel 1

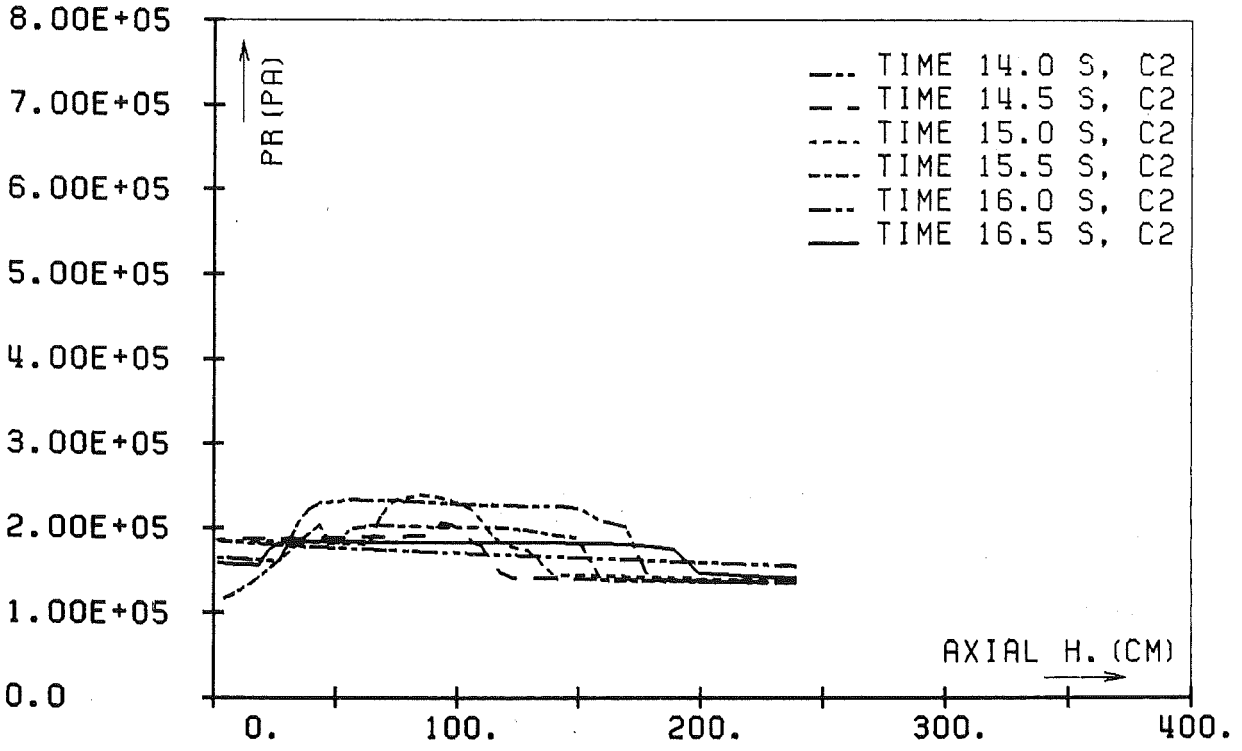

Fig. 20 : Axial pressure distribution, channel 2

V. Final remarks

The sodium boiling model as it has been incorporated into the SANDCMOT code is presented. A mixture flow concept is used to describe the two-phase flow. Thermodynamic equilibrium along the saturation line is assumed while a slip correlation is used to describe the different velocities of vapor and liquid phase. The model has been tested against the TREAT-R5 experiment /2/. The results are found encouraging although some deviations suggest further improvements. In the current form now, the SANDCMOT code is suitable for analysis of loss-of-flow accidents in LMFBR's up to fuel pin disintegration including sodium boiling and clad motion. As the code has a multichannel structure. Sodium boiling is treated in a two-dimensional way. Also, clad motion can be described within each channel.

VI. Appendix

VI.A Finite difference form of momentum equations

When the momentum equations of system (2.1e) are integrated over a certain control volume associated with the staggered (momentum) grid and the time derivative is replaced by a forward time difference the discretized form of the momentum equation is obtained. This is to be explained in more detail for the axial momentum equation. Let b = (k,j+1/2) denote the northern face of the control volume k,j and G_b be the axial component of the vector Γ at the northern boundary location. Let A_b be the area of this boundary surface and $DZ_{j+1/2}$ be the distance between midpoint (k,j) and (k,j+1). The adopted finite difference form to the momentum equation (2.1e) is

$$(AG^{n+1}-AG)_b/dt + \Sigma_{b'} n_{b'} (AG)_{b'}^{n+1/2} \langle x v_v + (1-x) v_l \rangle_{b'} / DZ_{j+1/2}$$

$$- A_b (p_{kj}-p_{kj+1})^{n+1}/DZ_{j+1/2} + A_b \rho_b g_z + f_w (AG)_b^{n+1} = 0 \qquad (A.1a)$$

The summation is to be performed over all boundary surfaces of the staggered grid control volume centered around (k,j+1/2). Consequently, the subscript b' runs over all duplets

$$b' := (k,j),\ (k,j+1),\ (k-1/2,j+1/2),\ (k+1/2,j+1/2) \qquad (A.1b)$$

Also, the time index n+1/2 appearing in the convective terms indicates that flow rates are taken both at the old and new time level. Except for $G_{k,j}$ and $G_{k,j+1}$ all G's are taken at the old time level. For the two exceptions an expansion around AG_b^{n+1}, b = (k,j+1/2), is used

$$AG_{k,j+1}^{n+1/2} = AG_b^{n+1} + 1/2 DZ_{j+1} (\delta AG/\delta z)_b = AG_b^{n+1} + R_{j+1}$$

$$AG_{k,j}^{n+1/2} = AG_b^{n+1} - 1/2 DZ_j (\delta AG/\delta z)_b = AG_b^{n+1} + R_j$$

Quantities without any time index are assumed at the old time level n.

Eq.(A.1a) can be cast into the following form

$$G_b = a_b + n_b d_b \Delta p_b^{n+1} \qquad \text{(A.1c)}$$

$$\xi = 1./dt + (\langle xv_v+(1-x)v_l\rangle_{k,j+1} - \langle xv_v+(1-x)v_l\rangle_{k,j})/DZ_{j+1/2} + f_w$$

$$d_b = (\xi DZ_{j+1/2})^{-1}$$

$$a_b = (A_b \xi)^{-1} (AG_b/dt - Conv - A_b r_b g_z)$$

$$Conv = \Sigma_b{}' \; n_b{}' R(AG)_b{}' \; \langle xv_v+(1-x)v_l\rangle_b{}'/DZ_{j+1/2}$$

where R(AG) indicates $AG_b^n{}'$ except for for the two cases noted above where the residuals R_{j+1}, R_j are meant. If j is replaced by j-1 the corresponding expressions for the southern boundary face are obtained.

A very similar derivation leads to the finite difference form of the radial momentum equation. However, three points are different here. First, the convective terms are all omitted for simplicity. This probably is of no major importance because radial flow rates usually are small. Second, as is explained in more detail in ref. /1/ compressibility effects are included into the radial pressure gradient in order to describe more correctly the time dependent pressure build-up when a radial mass flow sets in from one cell into another one. This procedure removes problems of exceedingly high radial flow rates if a time independent pressure gradient is used in the radial momentum equation. Third, the geometric quantities specifying the radial cross flow channels like cross flow area, channel length DR and hydraulic diameter all have to be given by input.

These notes should be sufficient to see how the finite difference form of the radial momentum equation is constructed and that it has a similar structure as eq.(A.1c).

VI.B Pressure matrix coefficients

The pressure equation (3.3e) essentially results from the mass equation when the the mass flow rates are expressed by help of the momentum equations and the density increments by the equations of state. The equations actually involved are

$$Vd\rho/dt_C + \Sigma_b\ n_b A_b G_b^{n+1} = 0 \qquad (B.1)$$

$$G_b^{n+1} = a_b + n_b d_b \Delta p_b^{n+1} \qquad (B.2)$$

$$d\rho_C = (R_p dp + R_h d\rho h + d\rho_T)_C \qquad (B.3)$$

$$d\rho h_C = dt/V\ (S_h + Vdp/dt_C - \Sigma_b\ n_b A_b G_b^{n+1} \langle h_f \rangle_b^{n+1}) \qquad (B.4)$$

$$S_h = Q_w + V\ \Sigma_b\ n_b (W_b \Delta p_b + q_b^{n+1})$$

The first two equations are identical to (3.3a,b). For convienience, the density increment has been brought into a general form. In case of two-phase flow the first two terms are as stated in (3.2c) while $d\rho_T$ is zero. In case of single phase flow R_p is identified with $\delta\rho/\delta p$ and R_h is zero. Furthermore, C is a short hand notion for (k,j). If (B.2) and (B.3) are substituded into (B.1) and use is made of (B.4) one finally may find

$$(\Lambda_C + \Sigma_b\ A_b d_b \zeta_b)\ p_C^{n+1} - \Sigma_b\ A_b d_b \zeta_b\ p_B^{n+1} = \Pi \qquad (B.5)$$

$$\Lambda_C = V(R_p + R_h)/dt_C$$

$$\zeta_b = 1 - R_{h,C} \langle h_f \rangle_b^{n+1}$$

$$\Pi = \Lambda_C p_C - R_h S_h - Vd\rho_T/dt - \Sigma_b\ n_b A_b a_b \zeta_b$$

Eq. (B.5) has the form of (3.3e) if β_C is identified with the term in brackets and β_B with $A_b d_b \zeta_b$.

VI.C Equations of state

Various equations of state are needed to set up the two-phase model. Here, those used for saturated sodium in liquid and vapor state will be given.

Saturation pressure (Pa)

$$PSAT(T) = 3.32445E9 \exp(-12020.46/T) \tag{C.1}$$

Saturation temperature (K)

$$TSAT(p) = 5220.42/(9.52172-\log_{10}(p)) \tag{C.2}$$

Saturated liquid density (kg/m^3)

$$\rho_l(T) = 1011.8 - 0.22054\ T - 1.9226E\text{-}5\ T^2 + 5.6371E\text{-}9\ T^3 \tag{C.3}$$

Saturated vapor density (kg/m^3)

$$\rho_v(T) = 1./SVOL(T) \tag{C.4}$$
$$SVOL(T) = \lambda(T)/(T\ \delta PSAT/\delta T) + 1./\rho_l$$

Saturated liquid enthalpy (J/kg)

$$h_l(T) = -7.1393E3 + 35.206\ T - 7.0513E\text{-}3\ T^2 + 2.5711E\text{-}6\ T^3 - 1.2428E5/T \tag{C.5}$$

Saturated vapor enthalpy (J/kg)

$$h_v(T) = h_l(T) + \lambda(T) \tag{C.6}$$

Heat of vaporization (J/kg)

$$T_{crit} = 2509.46\ K \tag{C.7}$$
$$\xi = 1. - T/T_{crit}$$
$$\lambda(T) = 1.82E5\ (-5.557012\ \xi + 31.25992\ \xi^{0.4}) \quad T < 1644.26\ K$$

$$\lambda(T) = 4.73773E6\ \xi^{0.32227} \qquad T > 1644.26\ K$$

Some other functions frequently needed are also summarized:

Liquid dynamic viscosity (kg/ms)

$$\mu_l(T) = 7.7266E\text{-}5\ \exp(851.236/T) \tag{C.8}$$

Vapor dynamic viscosity (kg/ms)

$$\mu_v(T) = -2.E\text{-}7 + 2.32E\text{-}8\ T \tag{C.9}$$

Liquid heat conductivity (W/mK)

$$k_l(T) = 109.74 - 0.0645\ T + 1.173E\text{-}5\ T^2 \tag{C.10}$$

Vapor heat conductivity (W/mK)

$$k_v(T) = 0.0181 + 2.74E\text{-}5\ T \tag{C.11}$$

Homogeneous mixture sound speed (m/s)

$$c_m^{-2} = \rho\ \{\alpha/(\rho_v c_v^2) + (1-\alpha)/(\rho_l c_l^2)\} \tag{C.12}$$

Most of the functions summarized above are taken from ref./21/.

VI.D Characteristics analysis

When the system of equations (2.1e) is considered in its one-dimensional version and the vector $\Omega = (p,v,\alpha)^T$ is taken to contain the dependent variables, expanding the derivatives will allow to cast the system of equations into the following form

$$A\ \delta/\delta t\ \Omega + B\ \delta/\delta x\ \Omega = 0 \qquad (D.1)$$

In above equation A and B are two 3×3 matrices that will be specified below. Also, friction and gravitational terms, heat input and fluid heat fluxes are not considered for reason of simplicity. Furthermore, the enthalpy equation has been transformed to an equation for entropy by the well known thermodynamic relation

$$Tds = dh + 1/\rho\ dp \qquad (D.2)$$

This equation is valid for either phase. The entropy s will depend on pressure p only because of the assumed saturation conditions within each phase. For brevity some short hand notations are appropriate. Let

$$\rho' = \alpha\rho_v S + (1-\alpha)\rho_l\ , \qquad \rho'' = \alpha\rho_v S^2 + (1-\alpha)\rho_l$$

$$c^{-2} = \alpha/c_v^2 + (1-\alpha)/c_l^2\ , \qquad c'^{-2} = \alpha S/c_v^2 + (1-\alpha)/c_l^2 + \alpha\rho_v S_p$$

$$d\rho = \rho_v - \rho_l\ , \qquad d\rho' = \rho_v S - \rho_l + \alpha\rho_v S_\alpha$$

$$d\rho'' = \rho_v S^2 - \rho_l + \alpha\rho_v 2SS_\alpha$$

$$(\rho s)' = \alpha S\rho_v s_v + (1-\alpha)\rho_l s_l$$

$$d\rho s = \rho_v s_v - \rho_l s_l$$

$$d\rho s' = \rho_v S s_v - \rho_l s_l + \alpha\rho_v s_v S_\alpha$$

$$c''^{-2} = \alpha S^2/c_v^2 + (1-\alpha)/c_l^2 + \alpha\rho_v 2SS_p$$

$$D^{-2} = \alpha/D_v^2 + (1-\alpha)/D_l^2$$

$$D'^{-2} = \alpha S/D_v^2 + (1-\alpha)/D_l^2 + \alpha\rho_v s_v S_p$$

$$c_i^{-2} = d\rho_i/dp \ , \qquad i = v,l$$

$$D_i^{-2} = d(\rho_i s_i)/dp$$

The convention is adopted that the symbols S_p and S_α denote partial differentiation of the slip function S with respect to p and α. These differentials occur because the slip S is interpreted as a function of p and α. The matrices A and B are as follows

$$A = \begin{bmatrix} c^{-2} & 0 & d\rho \\ v/c'^2 & \rho' & v\,d\rho' \\ D^{-2} & 0 & d\rho s \end{bmatrix}, \quad B = \begin{bmatrix} v/c'^2 & \rho' & v\,d\rho' \\ 1+v^2/c''^2 & 2v\rho'' & v^2 d\rho'' \\ v/D^2 & (\rho s)' & v\,d\rho s' \end{bmatrix}$$

The characteristic polynomial is obtained from $\det(A\lambda + B) = 0$, where λ is the characteristic. Evaluation of the determinant leads to a third order polynomial in λ:

$$\begin{aligned}
&(\lambda/c^2+v/c'^2)\cdot \\
&\{\rho' d\rho s(\lambda+2v\rho''/\rho')(\lambda+vd\rho s'/d\rho s) - (\rho s)' v d\rho'(\lambda+vd\rho''/d\rho')\} \\
&- \rho'\cdot \\
&\{(\lambda v/c'^2+v/c''^2+1)(\lambda d\rho s+vd\rho s') - (\lambda v d\rho'+v^2 d\rho'')(\lambda/D^2+v/D'^2)\} \\
&+ (\lambda d\rho+vd\rho')\cdot \\
&\{(\rho s)'(\lambda v/c'^2+v/c''^2+1) - (\lambda\rho'+2v\rho'')(\lambda/D^2+v/D'^2)\}
\end{aligned} \qquad (D.3)$$

This polynomial at least has one real root which in case of no slip (S=1) is $\lambda = v$. The question if there are two more real roots is hard to decide from above equation directly. Numerical investigations including for example the IBM FORMAC computer program /23/ may be appropriate. Such analysis has not been carried out, yet.

VI.E TREAT-R5 sample input

```
TREAT-R5 POST TEST CALCULATION, 7-PIN BUNDLE, 20% ENR. INNER PIN, 14% OUTER PINS
    2     3     0     0     3     1
        0.0          13.0                                                    TIMO,TFIN
        1.0                                                                  AOTEMP
        0.1           .25          .30         .28E7         1700.
START OF GEOMETRY INPUT
    4                                                                        # OF AXIAL SUBMODELS
FIRST AXIAL SUB-MODEL (SS LOWER REFLECTOR)
    1     4     1     0    10     4     1                                   10 RADIAL ZONES
        0.0          .1651                                                   AXIAL EXTENSIONS
    1     1     3     1     1     1     3     1     3     1                   HEAT TRANSFER FLAG
    3     2     0     2     3     2     0     0     0     0                   MECHANICS FLAG
    1     1     1     1     1     1     1     1     1     1                   # OF RADIAL REGIONS
    5     3     1     3     5     3     1     5     1     4                   # THERMAL NODES
    1     1     1     1     1     1     1     1     1     1                   # STRESS NODES
    3     3     4     3     3     3     4     3     6    14                   4-SODIUM, 6-HELIUM, 14-MOLYBDAN
    1    -1    -1     1     1    -1    -1    -1    -1    -2                   RADIAL CONNECTION FLAG
 7.498E-5    7.730E-5     2.17E-4        AFLOW
 4.515E-3    2.367E-3     5.61E-3        HDIAM
      1.0          1.0          1.0     HWPERIMETER
      0.0   9.5740E-3          0.0     INNER GRID RADIUS
      0.0   9.6700E-3          0.0     OUTER GRID RADIUS
    300.0                              TBOUND
    1.200
      0.0        .00247       .00254      .002921      .002921      .005692      .005692      .006152      .006222      .008679  RADII
  .008749       .009142      .009142       .01040       .01040       .01091       .01091      0.01372      0.01372      0.01524  RADII
      1.0          1.0          1.0          1.0          1.0       1.3450       1.3450       1.0820       1.0400       0.9618  CORF
   0.9811        1.080        1.080        1.050        1.050       1.0460       1.0460          1.0          1.0          1.0  CORRF
      0.0          0.0          0.0          0.0          0.0          0.0          0.0          0.0          0.0          0.0
      0.0          0.0          0.0          0.0          0.0          0.0          0.0          0.0          0.0          0.0
      0.0          0.0          0.0          0.0          0.0          0.0          0.0          0.0          0.0          0.0
      0.0          0.0          0.0          0.0          0.0          0.0          0.0          0.0          0.0          0.0  CRACKS
      .00          0.0          5.0          0.0          0.0          0.0          5.0          0.0          1.0          0.0  POROS.
     1.00          .00          0.0          0.0         1.00          0.0          0.0          0.0          0.0          0.0  PFRAC
    0     0     0     0     0     0     0     0     0     0                    NSHAPE
     594.          594.         594.         594.         594.         594.         594.         594.         300.         300.  TINIT
SECOND AXIAL SUB-MODEL (NUCLEAR HEATED FUEL PIN SECTION)
    2     1     1     0    10    22     1
   0.1651        1.0795
    1     1     3     1     1     1     3     1     3     1
    1     2     0     2     1     2     0     0     0     0                   MECHANICS FLAG
    1     1     1     1     1     1     1     1     1     1
    5     3     1     3     5     3     1     5     1     4
    1     1     1     1     1     1     1     1     1     1
    1     3     4     3     1     3     4     3     6    14                   4-SODIUM, 6-HELIUM, 14-MOLYBDAN
    1    -1    -1     1     1    -1    -1    -1    -1    -2                   (CONNECT)
 7.498E-5    7.730E-5     2.17E-4        AFLOW
 4.515E-3    2.367E-3     5.61E-3        HDIAM
      1.0          1.0          1.0     HWPERIMETER
      0.0   9.5740E-3          0.0     INNER GRID RADIUS
      0.0   9.6700E-3          0.0     OUTER GRID RADIUS
```

```
     300.0                                                TBOUND
     1.200
       0.0       .00247       .00254      .002921      .002921      .005692      .005692      .006152      .006222      .008679  RADII
   .008749      .009142      .009142       .01040       .01040       .01091       .01091      0.01372      0.01372      0.01524  RADII
       1.0          1.0          1.0          1.0          1.0       1.3450       1.3450       1.0820       1.0400       0.9618  CORF
    0.9811        1.080        1.080        1.050        1.050       1.0460       1.0460          1.0          1.0          1.0  CORRF
       0.0          0.0          0.0          0.0          0.0          0.0          0.0          0.0          0.0          0.0
       0.0          0.0          0.0          0.0          0.0          0.0          0.0          0.0          0.0          0.0
       0.0          0.0          0.0          0.0          0.0          0.0          0.0          0.0          0.0          0.0
       0.0          0.0          0.0          0.0          0.0          0.0          0.0          0.0          0.0          0.0  CRACKS
       .10          0.0          5.0          0.0          0.1          0.0          5.0          0.0          1.0          0.0  POROS.
      5.34          .00          0.0          0.0         4.75          0.0          0.0          0.0          0.0          0.0  PFRAC
  -3     0     0     0    -3     0     0     0     0     0                NSHAPE
       1.0         0.00   1.96274E04                                     RADIAL PROFILE FOR 20% ENRICHED CENTER PIN IN 7-PIN BUNDLE
       1.0    -0.22895     0.016790                                      RADIAL PROFILE OUTER RING (PARABOLA)
      594.         594.         594.         594.         594.         594.         594.         594.         300.         300.  TINIT
THIRD AXIAL SUB-MODEL (UPPER BLANKET + INCONEL)
   3     2     1     0    10     4     1
    1.0795       1.2446
   1     1     3     1     1     1     3     1     3     1
   3     2     0     2     3     2     0     0     0     0    MECHANICS FLAG
   1     1     1     1     1     1     1     1     1     1
   5     3     1     3     5     3     1     5     1     4
   1     1     1     1     1     1     1     1     1     1
   3     3     4     3     3     3     4     3     6    14    4-SODIUM, 6-HELIUM, 14-MOLYBDAN
   1    -1    -1     1     1    -1    -1    -1    -1    -2    (CONNECT)
 7.498E-5     7.730E-5     2.17E-4          AFLOW
 4.515E-3     2.367E-3     5.61E-3          HDIAM
       1.0          1.0          1.0          HWPERIMETER
       0.0    9.5740E-3          0.0          INNER GRID RADIUS
       0.0    9.6700E-3          0.0          OUTER GRID RADIUS
     300.0                                   TBOUND
     1.200
       0.0       .00247       .00254      .002921      .002921      .005692      .005692      .006152      .006222      .008679  RADII
   .008749      .009142      .009142       .01040       .01040       .01091       .01091      0.01372      0.01372      0.01524  RADII
       1.0          1.0          1.0          1.0          1.0       1.3450       1.3450       1.0820       1.0400       0.9618  CORF
    0.9811        1.080        1.080        1.050        1.050       1.0460       1.0460          1.0          1.0          1.0  CORRF
       0.0          0.0          0.0          0.0          0.0          0.0          0.0          0.0          0.0          0.0
       0.0          0.0          0.0          0.0          0.0          0.0          0.0          0.0          0.0          0.0
       0.0          0.0          0.0          0.0          0.0          0.0          0.0          0.0          0.0          0.0
       0.0          0.0          0.0          0.0          0.0          0.0          0.0          0.0          0.0          0.0  CRACKS
       0.0          0.0          5.0          0.0          0.0          0.0          5.0          0.0          1.0          0.0  POROS.
      5.34          .00          0.0          0.0         4.75          0.0          0.0          0.0          0.0          0.0  PFRAC
   0     0     0     0     0     0     0     0     0     0                NSHAPE
      594.         594.         594.         594.         594.         594.         594.         594.         300.         300.  TINIT
FOURTH AXIAL SUB-MODEL (UPPER PLENUM - HELIUM , CALC. FROM 0.5 IN3 GAS VOLUME)
   4     3     1     0    10    12     1
    1.2446       2.4376
   1     1     3     1     1     1     3     1     3     1
   0     2     0     2     0     2     0     0     0     0    MECHANICS FLAG
   1     1     1     1     1     1     1     1     1     1
   5     3     1     3     5     3     1     5     1     4
   1     1     1     1     1     1     1     1     1     1
   6     3     4     3     6     3     4     3     6    14    4-SODIUM, 6-HELIUM, 14-MOLYBDENUM
   1    -1    -1     1     1    -1    -1    -1    -1    -2    (CONNECT)
 7.498E-5     7.730E-5     2.17E-4          AFLOW
```

```
  4.515E-3    2.367E-3     5.61E-3       HDIAM
       1.0         1.0         1.0       HWPERIMETER
       0.0   9.5740E-3         0.0       INNER GRID RADIUS
       0.0   9.6700E-3         0.0       OUTER GRID RADIUS
     300.0                               TBOUND
     1.200
       0.0       .00247      .00254     .002921     .002921     .005692     .005692     .006152     .006222     .008679  RADII
   .008749      .009142     .009142      .01040      .01040      .01091      .01091     0.01372     0.01372     0.01524  RADII
       1.0         1.0         1.0         1.0         1.0      1.3450      1.3450      1.0820      1.0400      0.9618  CORF
    0.9811       1.080       1.080       1.050       1.050      1.0460      1.0460         1.0         1.0         1.0  CORRF
       0.0         0.0         0.0         0.0         0.0         0.0         0.0         0.0         0.0         0.0
       0.0         0.0         0.0         0.0         0.0         0.0         0.0         0.0         0.0         0.0
       0.0         0.0         0.0         0.0         0.0         0.0         0.0         0.0         0.0         0.0
       0.0         0.0         0.0         0.0         0.0         0.0         0.0         0.0         0.0         0.0
       2.0         0.0         5.0         0.0         2.0         0.0         5.0         0.0         1.0         0.0  POROS.
      5.34         .00         0.0         0.0        4.75         0.0         0.0         0.0         0.0         0.0  PFRAC
 0     0    0     0    0     0    0     0    0     0                NSHAPE
      594.        594.        594.        594.        594.        594.        594.        594.        300.        300.  TINIT
AXIAL POWER INPUT
  24     0     1.0     1.0
       0.0         0.0       .7316       .7858       .8346      .87756      .91443      .94495       .9689      .98614
    .99652        1.00       .99652      .98614      .96890      .94495      .91443      .87756       .8346      .78585
    .73164      .73160         0.0         0.0
       0.0       .1652       .1720       .2220       .2720       .3220       .3720       .4220       .4720       .5220
     .5720       .6220       .6720       .7220       .7720       .8220      0.8720      0.9220      0.9720      1.0220
    1.0720      1.0792      1.0796      2.4376
TIME DEPENDENT INPUT ... FLOW RATE...INLET PRESSSURE...PRESSURE DROP...TEMP...POWER
  5.1373E-4    11                                                  |||||||||| FLOW RATE IS M**3/SEC
       2.1         2.1         2.1         1.0         0.6        0.50        0.00        0.00        -1.0         0.0
       0.0
       0.0         1.0        7.95        10.0        11.0        13.7        14.5        17.8        18.0       19.35
      28.0
     1.0E0    10                                                  |||||||||| INLET PRESSURE IN ATM
      8.369       8.097        4.66       3.266       1.565      1.2248      1.1568        0.68       0.408      0.2722
       0.0        7.95         8.5         9.0        10.0        10.8        12.0        14.0        18.0        26.0
     1.0E0     2                                                 |||||||||| RETURN FLOW CHANNEL PRESSURE DROP
      -15.1       -15.9
       0.0        33.0
      1.E0     9                                                 |||||||||| PRESSURE DROP IN ATM, CALC. VIA FLOW RATE, DPHYD.
    -1.0817     -1.0817      -0.700       -0.38      -0.2667     -0.24632      -0.200      -0.200      -0.200
       0.0        7.95         9.0        10.0        11.0        13.7        14.5        19.0        33.0
    600.00     2                                                 ||||||||||  INLET TEMPERATURES
       1.0       1.030
       0.0        15.0
  7     0    5763.688                                            |||||||| COUPLING FACTOR FOR 20% UO2 OUTER RING 14%
  9
      0.10       0.020     6
      3.50       0.050    10
      5.20       0.005   100
      5.70       0.010    10
      7.95       0.050    10
     13.75       0.020    20
     19.00        .001    25
     22.00        .010     5
     28.00        .001   100
  3    12    26    33
```

```
MATERIAL PROPERTY INPUT      |||| MAT(11)=ARGON, MAT(12)=HELIUM
    5
    1
       0.0         .400
   11                                                    ||||||||| THERMO PROPERTIES FOR ARGON 0.35 ATM
       0.0          1.0          0.0          0.0
       0.0          0.0          0.0          0.0          0.0
    1.77E-2      1.77E-2          521.         521.         .624          .624
   12                                                    |||||||| THERMO PROPERTIES FOR HELIUM 3.5 ATM
       0.0          1.0          0.0          0.0
       0.0          0.0          0.0          0.0          0.0
     .14184       .14184         5238.        5238.         .624          .624
   13                                                    ||||||||| THERMO PROPERTIES FOR FUSED QUARTZ
      1708.        1709.          0.0          .01
       0.0          0.0          0.0          0.0
       1.88         2.59         1047.        1047.        2550.         2550.
   14                                                    ||||||||| THERMO PROPERTIES FOR MOLYBDENUM
      2890.        2892.         1000.          .01
       0.0          0.0          0.0          0.0
     110.0        110.0          251.0        251.0       10220.        10220.
GAP INPUT DATA
    2
    1     2     0     1     1     1     3
    8.25E-6     8.25E-6      1.22E5       5.0E07       1.7E04       1.7E04       0.1E00
   1.033E02    1.677E-1                                                          GAP GAS CONDUCTIVITY POLYNOMIAL
    2     0     0     1     1     1     3
    8.25E-6     8.25E-6      1.22E5       1.7E04       1.7E04       1.7E04       0.1E00
       1.0          0.0          0.0          0.0          0.0
CONVECTION HEAT TRANSFER DATA
    1     1     2
    3     3       50.00      1.0101
    1     4         0.0         0.0
PLENUM DATA
     594.26       1.E01
END OF SANDPIN INPUT
```

```
SODIUM BOILING AND CLAD MOTION INPUT (by NAMELIST statements)

 ***TREAT-R5 RECALCULATION WITH SANDCMOT  11/85                    **
 &REST
 KREST=0,NRFR=21,NRFW=22,NPLT=20,ISTPM=8888,ISTPI=100,             &END
 &SAND
 TFIN=16.95,DTYME(7)=1.E-3,NTYME(7)=100,                           &END
 &NAM0
 JLI=4,JUI=24,DZW=8*1.0,24*0.02,12*1.03,IMATM=3,                   &END
 &NAM1
 RENC1=1600.,FRICB=0.316,FRICE=-0.25,RENCR=2300.,
 FRICB1=0.046,FRICE1=-0.2,XNYFR=5.0857E-05,VOIDB=1.0E-3,
 NFRICO=3,FRFMAX=5.,PLENA=5.5,PLENZ=4.5,
 DHIN=3.81E-2,AINL=1.1395E-3,FRFIN=5.E6,FRFOU=5.1E6,
 FORIFI=1.0E4,FORIFO=4.0E4,PRGRD=100.,DPLOS=0.00,PBARO=1.0,        &END
 PRX=1.5,PMAS=8.E-1,IPLEN=1,ACMIN=1.E-8,                           &END
 &NAM2
 DR=5.3783E-3,1.0E5,1.E05, ACONC=1.376E-2,0.0,0.0,
 FRFR=1.,DOHR=2.E-3,FORIF=1.0,SGRD=0.0,SLIPM=30.,                  &END
 &NAM3
 FZIP=.0,A0=.5,B0=.0,CDTMIN=5.00E-4,CDTMAX=2.E-2,RELX=1.0,
 CDTBL=2.E-4,                                                      &END
 &WETT
 TETCF=1.574,TETCC=1.0466,DROPD=2.0E-3,                            &END
 &ENTR
 PENTR=2.0,WECR=13.0,TAURES=0.7E-3,DRPFRC=0.2,
 ADROP=1.169E-6,ADPMIN=1.0E-10,DNU1=0.,DNU2=0.5,DNU3=0.33,
 FENTRB=0.271,FENTRE=0.217,FUSURF=1.,EFRAC=1.,CENTR=1.0,           &END
 &THEM
 ZGAP=1.0E0,VMAX=1.00,SHEAT=1.00,PLENR=5.E4,Y1=0.00,
 Y2=15.,Y3=1.2E5,Y4=17.0000,HDROP=0.025E0,CPC=0.000,CVC=1.00,
 XNU1=0.,XNU2=.023,XNU3=.8,XNU4=.33,XNU5=.0,DTSUP=5.0,
 RDROP=1.2E-3,GAMR=1.0,DHDP=0.0,                                   &END
 &PLOT
 DTPL=1.E-2,TPLOT=70.0,NXX=0,JLPR=1,JUPR=45,DTWRIT=0.1101,
 DTCURV=5.0E-2,TCURV=0.0,TWRIT=0.44873,                            &END
 &DEBG
 IDBP=0,IDBT=0,IDUGR=2                                             &END
END OF BOILING AND CLAD MOTION INPUT
```

```
POWER HISTORY FOR TREAT-R5
        10   (ten data records to be read in)
               TIME                                ACCUMULATED ENERGY (MJ)
               0.100          0.000000E+00         0.000000E+00
               3.000                                       0.00
               3.200                                       0.40
               3.500                                       2.50
               4.000                                      32.50
               4.970                                     158.60
               5.200                                     174.70
               5.500                                     193.30
              17.000                                     912.05
              19.000                                    1042.05
              19.200                                    1046.05
END OF POWER TRACE INPUT
```

VII. Nomenclature

symbol	dimension	meaning
A	m^2	flow cross sectional area
b	-	index denoting control volume surface areas
c_p	J/kg/K	heat capacity
$c_{m,v,l}$	m/s	sound speed of mixture, vapor, liquid
C	-	centroid of control volume, e.g. (k,j)
d_h	m	hydraulic diameter
dt	s	time increment
DR	m	radial mesh length
DZ	m	axial mesh length
f	-	friction factor
F_w	N/m^3	friction force per unit of volume
g	m/s^2	gravitational acceleration
$G_{r,z}$	kg/m^2s	radial, axial mass flux density
h	J/kg	mixture enthalpy/mass
h_f	J/kg	mixture enthalpy/mass based on quality x
$h_{v,l}$	J/kg	enthalpy per unit of mass of vapor or liquid phase
k	W/mK	heat conductivity
l	m	length of pipe section
p	Pa	pressure
PSAT	Pa	saturation pressure
q_b	W/m^2	fluid heat flux
Q_w	W/m^3	power density
r	m	radial coordinate
$R_{p,h}$		coefficients in mass increment expression
t	s	time coordinate
T	K	temperature
TSAT	K	saturation temperature
u	m/s	radial velocity
v	m/s	axial velocity
W	m/s	velocity vector
x	-	vapor quality
z	m	axial coordinate

α	-	void fraction
β	-	coefficient in pressure matrix equation
δ	-	indicates partial differentiation
Δ	-	indicates finite difference
ϕ	W/m^2	heat flux pin to coolant
Γ	kg/m^2s	mass flux density vector, $\Gamma=(G_r,G_z)^T$
λ	J/kg	specific heat of vaporization
μ	kg/ms	dynamic viscosity
Ψ^2	-	Lockhart-Martinelli parameter
ρ	kg/m^3	density

Indices

ex	bundle exit
in	bundle inlet
j	axial node index
k	radialnode index
l	liquid
m	mixture
n	time index
sp	single phase
tp	two phase
v	vapor
w	wall
sat	saturation

VIII. REFERENCES

1. P. R. Henkel, 'Hüllrormaterialbewegung während eines Kühlmitteldurchsatzstörfalls in einem schnellen, natriumgekühlten Reaktor', KfK 3967 (1985)

2. M.A. Grolmes et.al., 'R-Series Loss-Of-Flow Safety Experiment In TREAT', Proc. Conf. Fast Reactor Safety, CONF-740401, Beverly Hills, California, 1, 279 (1974)

3. P.K. Mast, 'SANDPIN', unpublished, Sandia National Laboratories, Albuquerque, NM, USA

4. M. Bottoni, D. Struwe, 'BLOW-3A, A Theoretical Model to Describe Transient Two-Phase Flow Conditions in LMFBR Coolant Channels', KfK 3317 (1984)

5. D. Chrisholm, 'Void Fraction During Two-Phase Flow', J. Mech. Engng. Sci., 15, 3, (1973)

6. A.E. Bergles, J.G. Collier, J.M. Delhaye, G.F. Hewitt, F. Mayinger, 'Two-Phase Flow and Heat Transfer in the Power and Process Industries', Hemisphere Publishing Corporation (1981)

', 7. J. Loomis, W.H. Reed, A. Schor, H.B. Stewart, L. Wolf, 'THERMIT: A Computer Program for Three-Dimensional Thermal-Hydraulic Analysis of Light-Water-Reactor Cores',. EPRI NP-2032, (1981)

8. A.Y. Gunter, W.A. Shaw, 'A General Correlation of Friction Factors for Various Types of Surfaces in Crossflow', ASME Transactions, 67, p. 643, (1945)

9. M. Pilch, P.K. Mast, 'PLUGM, A Coupled Thermo-Hydraulic Computer Model for Freezing Melt Flow In a Channel', NUREG/CR-3190, SAND 82-1580, (1984)

10. A.L. Schor, N.E. Todreas,h Liquid Metal Boiling Working Group, Proceedings 10th Liquid Metal Boiling Working Group, Karlsruhe, Germany, Vol 1, 1, (1983)

11. H.K. Forster, N. Zuber, 'Dynamics of Vapor Bubbles and Boiling Heat Transfer', AIChE J. 1 (4) (1955)

12. J.C. Chen, 'A Correlation for Boiling Heat Transfer to Saturated Fluids in Convective Flow', ASME paper 63-HT-34, (1963)

13. R. B. Bird, W.E. Stewart, E.N. Lightfoot, 'Transport Phenomena', John Wiley & Sons (1960)

14. D. Moxon, Proceedings 10th Liquid Metal Boiling Working Group, Karlsruhe, Germany, Vol 1, 75, (1983)

15. J. Costa et.al., Proc. Fast Reactor Safety Meeting, Beverly Hills, California, CONF 740401, P3, p. 1202, (1974)

16. R.W. Lyczkowski, D. Gidaspow, C.W. Solbrig, E.D. Hughes, Nucl. Sci. Eng., 66, 378, (1978)

17. H.B. Stewart, B. Wendroff, 'Two-Phase Flow: Models and Methods', J. Comp. Physics, Vol. 56, No. 3, (1984)

18. A.M. Tentner, H.U. Wider, 'Pressure Drop Modeling in Variable Area, Multiphase Transient Flow', Multiphase Transport, Vol.2, p. 1137, T. N. Veziroglu, Ed., Hemisphere Publishing Company, Washington (1980)

19. P. Schmuck, Nucl. Techn. Vol.71, 314, (1985)

20. S.V. Patankar, 'Numerical Heat Transfer and Fluid Flow', Hemisphere, McGraw-Hill , New York, (1980)

21. J.K. Fink, M.G. Chasanov, L. Leibowitz, ANL-CEN-RSD-82-2, Argonne National Laboratory, (1982)

22. P. Henkel, 'SANDCMOT user instructions', KfK report, in preparation (1987)

23. J. Xenakis, 'PL/1-FORMAC Symbolic Mathematics Interpreter', 360-D03.004, IBM Corporation (1969)